Published in final edited form as:
Pain. 2014 August ; 155(8): 1632–1648. doi:10.1016/j.pain.2014.05.015.

Brain mediators of the effects of noxious heat on pain

Lauren Y. Atlas[1,*], **Martin A. Lindquist**[2], **Niall Bolger**[3], and **Tor D. Wager**[4]

[1]Department of Psychology, New York University, New York, NY, 10003

[2]Department of Biostatistics, Johns Hopkins University, New York, NY, 21205

[3]Department of Psychology, Columbia University, New York, NY, 10027

[4]Department of Psychology and Neuroscience, University of Colorado, Boulder, Boulder, CO 80309

Abstract

Recent human neuroimaging studies have investigated the neural correlates of either noxious stimulus intensity or reported pain. While useful, analyzing brain relationships with stimulus intensity and behavior separately does not address how sensation and pain are linked in the central nervous system. In this paper, we used multi-level mediation analysis to identify brain mediators of pain—regions whose trial-by-trial responses to heat explained variability in the relationship between noxious stimulus intensity (across four levels) and pain. This approach has the potential to identify multiple circuits with complementary roles in pain genesis. Brain mediators of noxious heat effects on pain included targets of ascending nociceptive pathways (anterior cingulate, insula, SII, and medial thalamus) and also prefrontal and subcortical regions not associated with nociceptive pathways *per se*. Cluster analysis revealed that mediators were grouped into several distinct functional networks, including: a) somatosensory, paralimbic, and striatal-cerebellar networks that increased with stimulus intensity; and b) two networks co-localized with 'default mode' regions in which stimulus intensity-related *decreases* mediated increased pain. We also identified 'thermosensory' regions that responded to increasing noxious heat but did not predict pain reports. Finally, several regions did not respond to noxious input, but their activity predicted pain; these included ventromedial prefrontal cortex, dorsolateral prefrontal cortex, cerebellar regions, and supplementary motor cortices. These regions likely underlie both nociceptive and non-nociceptive processes that contribute to pain, such as attention and decision-making processes. Overall, these results elucidate how multiple distinct brain systems jointly contribute to the central generation of pain.

[*]Corresponding author: Lauren Atlas, New York University, Meyer Hall, 6 Washington Place, Room 877, New York, NY 10003, Phone: 212-998-3720, laurenatlas@nyu.edu.

The authors declare no conflicts of interest.

Keywords

fMRI; mediation; neuroimaging; nociception; pain; connectivity; human

The relationship between stimulus intensity and perception is lawful and robust in all perceptual domains, including pain [2; 72]. However, while higher stimulus intensities usually lead to greater pain, there is nearly always variability in the stimulus-response relationship. Pain perception is strongly influenced by spontaneous fluctuations in arousal and attention [14; 46; 62], stimulus history [12; 37; 64], and other factors. Thus, a given stimulus intensity can be perceived or reported as painful or non-painful depending on brain activity prior to [14; 62], during [63], or after noxious stimulation [9; 44]. The purpose of the present study was to examine how variations in noxious stimulus intensity are transformed into variations in pain, focusing specifically on responses during noxious stimulation itself. In particular, we sought to identify regions that mediate stimulus effects on pain and those that do not respond strongly to noxious stimuli, but nonetheless play supporting roles in pain genesis.

Targets of spino-thalamo-cortical nociceptive pathways [32] and other nociceptive pathways (e.g., spino-parabrachial and spino-reticular; [83]) reliably track the stimulus intensity of painful events in human neuroimaging studies, including somatosensory (SI/SII), dorsal posterior [dpINS], anterior insular [aIns], and anterior cingulate [aCC] cortices and thalamus [5; 35; 60]. There is broad consensus that these ‘intensity coding’ regions also generally correlate with pain [25; 76], though the stimulus-response function between brain response and pain report may differ depending on the region [15; 20; 38; 48; 63].

However, only a few studies have directly compared brain activity related to stimulus processing with activity related to pain, and findings are mixed on which areas are most strongly associated with each. One seminal study found that dpINS correlated preferentially with stimulus intensity and aIns correlated preferentially with perceived pain [29], whereas another study found the opposite [6]. In addition, these previous studies do not provide models of how stimulus-related brain activity and pain-related brain activity are linked. While these studies identify correlates of *either* noxious stimulus intensity or pain perception, we know little about the brain processes that transform stimulus processing into pain, and which processes might contribute to pain independent of stimulus processing.

We used whole-brain multi-level mediation analysis [7; 80; 81], a linear multivariate approach that relates stimuli, brain responses, and behavior in a single model, to understand the pathways that mediate the effects of noxious input on pain perception. We identify three classes of relevant brain processes: 1) mediator regions that link stimulus intensity with pain; 2) thermosensory regions that respond specifically to noxious input; and 3) pain-related regions that contribute to decisions about pain above and beyond the linear and nonlinear effects of noxious stimulus intensity and thus may reflect endogenous decision-making processes that contribute to variations in pain, such as arousal, attention, and magnitude estimation. We identify networks with distinct functional properties related to pain genesis, which could help create a clearer picture of the multiple systems involved in

creating pain. This approach could also serve as a model for understanding sensory decision-making in other perceptual modalities.

Materials and Methods

Participants and Procedure

Participants—Thirty healthy, right-handed participants were enrolled in the study. Participants were recruited from the New York metropolitan area through posted flyers, advertisements on Craigslist, and if they had previously participated in studies in our lab and volunteered to be contacted for future research. All participants provided informed consent in accordance with the Declaration of Helsinki, as approved by the Columbia University Institutional Review Board. Preliminary eligibility was assessed with a general health questionnaire, a pain safety screening form, and an fMRI safety screening form. Participants reported no history of psychiatric, neurological, or pain disorders. Three participants completed calibration but were not scanned due to technical problems with the heat equipment (two participants) or discomfort with the MR environment (one participant). The fMRI imaging sequence was incorrect for one additional participant, leaving a final sample of twenty-six participants (nine female, mean age = 27.8, range: 20y - 50y).

Thermal stimulation and pain ratings—Thermal stimulation was delivered to the volar surface of the left (non-dominant) inner forearm using a 1 × 16 mm Peltier thermode (Medoc, Inc.). Each stimulus lasted 10 seconds, with 1.5-second ramp-up and ramp-down periods and 7 seconds at target temperature. Temperatures were individually calibrated for each participant using an adaptive staircase procedure. During calibration and during the fMRI portion of the experiment, participants rated stimulation on a continuous scale from 0-8 (0 = no sensation; 1 = non-painful warmth; 2 = low pain; 5 = moderate pain; 8 = maximum tolerable pain). This scale has been used in previous studies in our lab [7; 8], and provides measures of pain threshold and tolerance. It is similar to the 0-5 scale used by Bornhovd [15] and Buchel [20] but provides a broader range to increase sensitivities to subtle variations in perception. We used a continuous visual analogue scale (VAS) during fMRI scanning which provided further sensitivity to small-fluctuations in pain.

The calibration procedure allowed us to derive each participant's stimulus-response curve for the relationship between applied thermal stimulation and reported pain and to identify sites on the forearm with similar nociceptive profiles (i.e. the three with the lowest average residuals based on the predicted stimulus-response function). During the fMRI experiment, heat was applied to the three sites that responded most similarly to changes in temperature, and temperatures were selected for each individual based his or her dose-response curve. IRB restrictions precluded us from applying temperatures higher than 48°C, so all participants were required to have maximum tolerable pain levels fall within the range of 42–48°C. One participant exceeded this range (maximum predicted temperature based on calibration = 50°C) but was included in the experiment and received a maximum stimulus of 48°C. No participants reported maximum tolerable pain that fell below 42°C.

fMRI task design—fMRI images were acquired during 6 functional runs (8 trials/run, 48 trials). The thermode was placed on a different skin site for each run, with two total runs per

skin site. Task design is shown in Figure 1. At the start of each trial, a square appeared in the center of the screen for 50 ms, followed by a pair of faces from the Ekman set [34]. An emotional expression (Happy or Fearful) was presented for 33 ms, masked by a neutral face presented for 1467 ms. Face cues were evenly crossed with temperature.

As the conceptual focus of the present paper concerns the mechanisms that link changes in temperature with changes in pain, our mediation analyses collapse across the face cues to examine pain-evoked responses during noxious stimulation period as a function of temperature. To test whether face primes were ignorable here, we controlled for the effects of face cues (main effects and interactions with temperature) on regions identified in our mediation analysis. This assessed the possibility that masked emotional faces induced variability in the temperature-pain relationship. No main effects of face primes were found on the regions we report here, and all results reported were significant controlling for face prime identity; thus, we do not report priming effects in detail. A full analysis of the face primes is awaiting replication and extension in future experiments, and is not the main focus of this paper.

Cue presentation was followed by a six-second anticipatory interval during which a fixation cross was presented on the screen. Thermal stimulation was then delivered via the thermode for ten seconds (1.5s ramp up from baseline (32°C), 7s at peak destination temperature, 1.5s return to baseline) at levels calibrated to elicit ratings of non-painful warmth (VAS rating = 1; M = 40.8°C, SD = 2.03), low pain (VAS rating = 3; M = 43.1°C, SD = 2.10), medium pain (VAS rating = 5; M = 45.1°C, SD = 1.79), or high pain (VAS rating = 7; M = 47.0°C, SD = 1.14). Following thermal stimulation, a fixation cross was presented for a fourteen-second fixed inter-stimulus interval (ISI). The words “How painful?” then appeared on the screen for four seconds above an 8-point VAS. Participants rated the pain evoked by the preceding stimulus using an fMRI-compatible track-ball (Resonance Technologies, Inc.) with resolution equivalent to the screen resolution (i.e., approximately 600 discrete values between 1 and 8). The delay between pain offset and rating was included in order to maximize our ability to isolate pain-period responses using single-trial analysis. A 10-second ISI separated the rating period from the start of the next trial.

In this report, we focus on brain responses evoked during the 10-second thermal stimulation period. Anticipatory responses and responses during the pain rating period were analyzed and reported for a subset of participants, along with heat-evoked responses, in a separate paper [78] that used qualitatively different methods (pattern classification, rather than mediation analysis) and thus provide complementary findings.

Behavioral analyses—Behavioral data were analyzed using custom code implementing a linear mixed-effects model in Matlab software (MathWorks, Natick, MA), and verified using the Mixed procedure in SAS 9.1 (SAS Institute Inc., Cary, NC, USA). We modeled within-subjects effects of Temperature and Masked Emotion prime on pain report, as well as the Temperature x Masked Emotion interaction. To test for nonlinear effects of temperature on pain, we log-transformed temperatures and ratings and tested a linear mixed-effects model in log space.

FMRI acquisition and preprocessing

Imaging acquisition—Whole-brain fMRI data were acquired on a 1.5T GE Signa Twin Speed Excite HD scanner (GE Medical Systems) at Columbia University's Program for Imaging in Cognitive Science. Functional images were acquired with an echo-planar imaging sequence (TR = 2000ms, TE = 34 ms, field of view = 224 mm, 6 × 64 matrix, 3.5 × 3.5 × 4.0 mm voxels, 29 slices). Each run lasted 6 minutes and 18 seconds (189 TRs). Stimulus presentation and data acquisition were controlled using E-Prime software (PST Inc.).

Preprocessing—Prior to preprocessing, we identified global outlier time points by computing both the mean and the standard deviation of values in each image for each slice. Mahalanobis distances for the matrix of mean values (one per slice) × functional volumes were computed, and images with a value above 3 standard deviations were considered outliers. The same procedure was used for standard deviation values. Outlier time points were modeled as indicator vectors at the level of single trial estimation (see below, “Single trial analysis”). We also used principal components analysis (PCA) as an approach to noise reduction, using methods similar to previous work [74; 75]. In brief, standard PCA was used to define ten components expressed across the brain. A task-related design matrix was created using the timing of the fMRI paradigm: Cue, heat, and rating onsets were modeled with boxcars representing event duration and convolved with SPM's canonical hemodynamic response function plus time and dispersion derivatives. A nuisance-related design matrix was also constructed from the timeseries of global outlier timepoints and motion parameters. For each run, task- and nuisance-related predictors were regressed on each component time series, which provided correlation coefficients for how nuisance-related or task-related each component was. The ratio between correlation coefficients was used as a first step in determining whether each component was artifactual and should be removed: No components were removed that had a task-related R^2 value greater than 0.1, or whose ratio of nuisance-to-task was less than 2.0. Components that fit these criteria were then visualized both spatially (pattern of weights across voxels) and temporally (average activity across time). Trained research assistants carefully inspected the components, and only removed components that were clearly artifactual (e.g., those expressed only at the edge of the brain, those that included an obvious single spike, etc.). An average of 1.09 components per run was removed per subject (*SD* = 0.69).

Following PCA denoising, functional images were slice-acquisition-timing and motion corrected using FSL (FMRIB's Software Library; http://www.fmrib.ox.ac.uk/fsl/). Structural T1-weighted images were coregistered to the first functional image for each subject using an iterative procedure of automated registration using mutual information coregistration in SPM5 (Wellcome Trust Centre for Neuroimaging, London, UK) and manual adjustment of the automated algorithm's starting point until the automated procedure provided satisfactory alignment. Data were smoothed with an 8mm-FWHM Gaussian smoothing kernel using SPM5.

Structural images were normalized to MNI space using a genetic algorithm (GA) based normalization. This approach is a refinement of the standard SPM5 warping and improves

inter-subject registration, and is described in detail in [7]. We note that because we started with a group mean registered to MNI space, the resulting warped images were still registered with MNI space. Normalized functional images were interpolated to 2×2×2 mm voxels.

FMRI analysis

Single trial analysis—We used single trial analysis to elicit a measure of brain response (i.e. area under the curve) to each trial, in each voxel, for each subject. Our method is described in detail in [7]. In brief, we quantified single-trial response magnitudes by constructing a GLM design matrix with separate regressors for each trial, as in the "beta series" approach of Rissman et al. [67]. However, we used a flexible basis set to model each trial, thus allowing the shape of the modeled HRF to vary across trials and voxels. The basis set consisted of three curves shifted in time and was customized for thermal pain responses based on previous studies [47]. The positions of the three basis functions were fixed in time relative to trial onset, and we allowed amplitude to vary in order to construct a fitted response on each trial. We evaluated the height, duration, delay-to-peak, and area under the curve (AUC) of each trial-wise fitted response. We chose to use the AUC of each fitted response (for each trial within each voxel) as a summary estimate of pain-period activity, as noxious heat has been shown to influence not only amplitude but also the duration of the evoked HRF [47], and thus the AUC captures these joint effects better than standard beta regressor amplitudes. When using a single-trial approach, it is common for some trials to be contaminated by movement or other artifacts. To mitigate such artifacts, we calculated trial-by-trial variance inflation factors (VIFs; a measure of design-induced uncertainty due in this case to collinearity with nuisance regressors). Any trials with VIFs that exceeded 2 or whose whole-brain AUC estimates exceeded 3 standard deviations from the mean were excluded from subsequent analyses (M = 2.69, SD = 2.07, range: 0-7 trials per participant).

Mediation analysis—We used whole brain multi-level mediation to examine the relationship between trial-by-trial changes in temperature (X), heat-evoked responses within a voxel (M), and reported pain (Y), as illustrated in Figure 1. Our methods have been described in detail in previous work [7; 80; 81]. The mediation approach is complementary to recent attempts to develop pain-predictive brain patterns using machine learning [16; 18; 52; 66; 78]. Whereas machine learning integrates activity across many regions into patterns that predict a single outcome variable (e.g. pain reports), the present multivariate approach relates responses within voxels to both noxious input *and* pain. We then address the complexity of these relationships by identifying multiple networks that make separate contributions to pain (see "Network analysis", below).

The mediation analysis presented here includes the following tests: 1) Whether changes in temperature influence activation within a voxel (measured by AUC) during heat (Path *a*); 2) Whether heat-evoked responses are correlated with pain reports, controlling for temperature (Path *b*); and 3) Whether the overall relationship between temperature and pain report (Path *c*) decreases when controlling for heat-evoked responses within a voxel (c-c', equivalent to $a*b+cov(a,b)$). This final test is a test of mediation. The interpretation of a mediator is that there is an indirect pathway through this region that links changes in external stimuli with

subjective responses, and that if a mediator were disrupted, the stimulus-response relationship would be diminished or abolished entirely.

We used bootstrap tests to test the significance of the mediation effect and each individual path. Bootstrap testing provides a more sensitive test of mediation than the Sobel test [13; 33; 71; 73]. We tested the significance of all effects (*a*, *b*, and *a*b*) using a bias-corrected, accelerated bootstrap [33]. We estimated distributions of subject level path coefficients by randomly sampling with replacement 10,000 observations (rows) from the matrix of [*a b a*b*] path coefficients for each voxel. Two-tailed, uncorrected p-values were calculated from the bootstrap confidence interval.

Multi-level mediation analysis incorporates a critical component, not present in single-level mediation, that offers a novel perspective on the relationship between within- and between-subject effects: The mediation effect (the decrease in the behavioral relationship when controlling for a mediator) is driven by a combination of consistent effects (Paths *a* and *b*) across a group of subjects and by *covariance* between Paths *a* and *b* across individuals [39] —i.e., the individuals that show strongly positive Path *a* effects also show strongly positive Path *b* effects, and vice versa. This implies that a region can mediate the relationship between independent and dependent variables either because it is used in similar ways by all subjects (e.g. the region shows increases with temperature [Path *a*] and greater activation predicts higher pain controlling for temperature [Path *b*]) or because individuals vary in consistent ways across Paths *a* and *b* (e.g. for subjects who show increases with temperature, greater activation predicts higher pain, and for subjects who show decreases with temperature, less activation predicts higher pain). The notion of mediation driven by covariance is relevant because individuals vary in the magnitude of pain they report with a given stimulus temperature in meaningful ways [24; 56; 84]. These person-level differences are often likely to be psychologically meaningful; for instance, individuals may use different strategies to cope with pain.

To examine whether mediation was driven by consistent effects across the group or by covariance between temperature effects and pain-related responses, we identified clusters that showed evidence of mediation, and extracted trial-wise data from each subject within each cluster. We then tested whether there were significant effects across the group in Paths *a* and *b* (i.e. whether there was a consistent group effect, essentially identical to what would be found with a standard one-sample t-test on Path *a* or Path *b* coefficients), or whether there were significant correlations between *a* and *b* coefficients across individuals. The former are reported as mediators that show consistent effects, while the latter are reported as driven by covariance and are likely to reflect psychologically meaningful individual differences, though identifying the sources and psychological correlates of these individual differences likely requires large-sample studies and is beyond the scope of the present report.

Thresholding—All results are false discovery rate (FDR) corrected at $q<0.05$, which corresponds to a voxel-wise threshold of $p < 0.001$ for the mediation effect, and a threshold of $p < 0.003$ for the conjunction across all three maps (*a*, *b*, *a*b*). We imposed a cluster extent threshold of 3 voxels at the lowest threshold. Network analyses and cluster-wise tests

were performed on data extracted from these voxels along with any contiguous voxels at uncorrected thresholds of $p < 0.005$ and $p < 0.01$.

We were specifically interested in characterizing responses within regions classically associated with pain-related processing [5; 35; 60]. We used an independent localizer to identify PPBN regions of interest (ROIs), using methods similar to [7]. In brief, we used a mega-analytic approach to compare high versus low intensity thermal stimulation across four different studies from our lab (n = 114). Voxels that showed a significant [high – low intensity] effect on the basis of family-wise error correction ($p < .05$) using Gaussian Random Fields as implemented in SPM5 (see Figure 1B) were defined as the pain-processing brain network (PPBN). Anatomical localization was determined based on the LONI Probabilistic Brain Atlas [70]. This revealed the following regions as comprising the PPBN (see Figure 1B): Bilateral superior, inferior, and middle frontal gyrus; bilateral precentral gyrus; right middle and bilateral lateral orbitofrontal gyrus; bilateral postcentral gyrus; bilateral supramarginal gyrus; bilateral superior and middle temporal gyrus; right hippocampus; right parahippocampal gyrus; left lingual gyrus; bilateral insular cortex; bilateral cingulate gyrus; bilateral caudate; bilateral putamen; brainstem; cerebellum, bilateral thalamus, and medial thalamus. For each path, we report results from ROIs that fell within the PPBN localizer, as well as regions outside the *a priori* PPBN.

Relationship to stimulus versus report—We tested for selectivity to temperature effects or variations in pain report by identifying voxels that were activated by temperature but unrelated to variations in report (i.e. showed Path *a* effects but neither Path *b* effects nor mediation), and voxels that showed the reverse relationship (Path *b* effects but neither Path *a* effects nor mediation). To ensure specificity to one process over the other, we identified voxels that showed significant effects in one path at $p < .001$, and whose p-values for the other path effect and the mediation effect exceeded $p > .05$ uncorrected.

Within Path *b* regions, we also tested for specificity to pain report and independence from nociceptive responses by testing whether brain regions predicted pain controlling for temperature as well as brain responses in mediators that fell within the boundaries of the PPBN. Trial-by-trial AUC estimates were averaged across PPBN mediator regions and included as covariates in multilevel mediation analyses for each Path *b* region (activation averaged across all voxels). This in turn allowed us to test the relationship between brain response and pain report controlling for both temperature and PPBN mediator response. Results are reported in Table 2.

Network analysis—We used dimension-reduction with non-metric multi-dimensional scaling (NMDS) and clustering to test whether mediator regions grouped into separate networks, using a multi-subject extension of methods described in previous work [40; 79]. We extracted the entire series of trial AUC estimates for each subject for each voxel within each mediator region. The goal was to provide a reasonable estimate of which voxels were grouped into coherent parcels (contiguous regions) and how these regions grouped into functional networks. A detailed explanation of the steps is below; in addition, the code for the analysis is available on our website (http://wagerlab.colorado.edu/tools). The function

parcel_clusters.m in the CANlab Core Tools package implements the three major steps described below, and visualized in Figure 2:

1. Dimension reduction

   Clustering of multivariate data is most stable when the data is not sparse, i.e., the dimensionality is low relative to the number of observations. To limit the dimensionality of the data, a spatio-temporal dimension-reduction step is first performed on the [$n \times v \times N$] data matrix of AUC data for n trials × v voxels × N participants (here, n = 48 trials [usually], v = 17,112 voxels , and N = 26 participants). A temporal data reduction is first performed to identify components with correlated AUC trial time series within each participant, followed by a spatial reduction to identify components with correlated spatial patterns across subjects. First, the [n × v] matrix of AUC data for each participant was subjected to PCA, using the [v × v] correlation matrices. Based on the scree plots across subjects, we saved the first 7 eigenvectors (spatial maps). These eigenvectors explained 74 +- 2.5% (st. dev. across subjects) of the variance in the full dataset. These eigenvectors were scaled by their variances (eigenvalues) and concatenated across subjects to form an [v × N*7] matrix of eigenvectors. This matrix was subjected to a second (across participant) PCA step to identify components with similar spatial maps across participants. We retained 12 eigenvectors (maps) based on the scree plot, which explained 65% of the variance across individuals. Component scores in this space were used for clustering. This is a data reduction step, and the results are not expected to depend strongly on the number of eigenvectors retained at either step, as long as most of the variance in the data is explained.

2. Parcellation

   Hierarchical agglomerative clustering with average linkage was used to group voxels into parcels--sets of contiguous voxels with similar profiles--in the [$v \times 12$] matrix of component maps. The goal of parcellation was to reduce the space from voxels to parcels (regions) for non-metric multidimensional scaling (NMDS)-based clustering of regions, so that NMDS is computationally tractable. Voxels whose trial AUC time series did not correlate with that of other voxels in the same parcel at $p < .001$ (in a random effects analysis across participants) were pruned from each parcel. Out of 140 parcels total, 127 parcels with more than 3 voxels after pruning were retained for subsequent analysis.

3. NMDS and clustering

   Parcels were now treated as the unit of analysis, and the AUC trial time series data were extracted from each parcel for each subject. Values in the [*n trials* × *parcels* × *N subjects*] data matrix were z-scored within participant to remove inter-subject differences in scaling, then concatenated into an [n*N × parcels] data matrix. Correlations among parcels were converted into a [parcels × parcels] matrix of distances using the formula $distance = (1 - r) / 2$. The NMDS stress plot (which operates on ranked distances and is therefore more robust to outliers and does not require a strictly Euclidean distance space) was examined and 7 dimensions (which

explained 79% of the variance in distances) were retained for the final cluster analysis.

Hierarchical agglomerative clustering with average linkage was used to cluster the parcels in this space into interconnected networks with correlated AUC trial time series. To choose the number of clusters in the final solution (*k*), for every possible choice of clusters between k = 2 and 20, we compared the cluster solution to the average and standard deviation of 1,000 clustering iterations with permuted parcel time series. This yielded a Z-score ([actual solution - mean permuted solution] / standard deviation) of permuted solution for each value of k. The best solution was k = 13, with a value of Z = 5.57 compared to the null-hypothesis single-cluster solution ($p < .0001$).

We report results from the solution that divided parcels into thirteen networks. Two networks consisted solely of parcels in white matter and were excluded from the results reported below. For each network, we averaged over in-network voxels for each subject and used multilevel mediation to test whether average network responses mediated temperature effects on pain.

Accounting for potential nonlinearities—Recent work demonstrates that noxious stimulus effects on brain responses may be nonlinear with respect to temperature [38] and that some regions show nonlinear relationships with respect to pain [15; 19; 48]. Nonlinearities in the relationship between temperature and pain are one of the effects that decouple stimulus intensity from reported pain, along with others (sequence and learning effects, attention, and variance related to decision-making processes). Our primary analysis controlled for linear effects of stimulus intensity when assessing the brain relationship with pain (Path *b*), which allows nonlinear effects of temperature to drive some Path *b* effects. In additional analyses, we ruled out potential non-linear influences of temperature: We assessed Path *b* (reported pain) and mediation effects controlling for temperature in a nonparametric fashion by including covariates for all possible differences among the four discrete levels of heat. To do this, we evaluated a second mediation where the input variable ("X") reflected the difference between the top two temperatures and the bottom two temperatures (e.g. [1 1 -1 -1] across the vector of [High pain, Medium pain, Low pain, Warmth] conditions) and we also modeled covariates for the difference between High and Medium conditions and Medium and Low conditions. This controls for any pairwise differences because any systematic linear or nonlinear differences among intensity levels can be modeled as a linear combination across these three regressors. The results of these tests are reported in Tables 2 and 3. Path *b* effects on all regions remained significant after controlling for non-linear effects of stimulus intensity.

Relationship to masked emotion face cues—The primary focus of this paper was to introduce a method to isolate the brain regions that link changes in noxious input to changes in pain perception. While our design included masked presentations of face stimuli with happy or fearful expressions, isolating the effects of the faces themselves on brain responses was outside the scope of this manuscript. However, mediation analysis takes advantage of the variability in the temperature-to-pain relationship, and given our experimental design,

some proportion of this variance might relate to the emotion face primes. To account for this possibility, Masked Emotion and Emotion × Temperature interactions were included as covariates in follow-up analyses for regions that showed significant Path *b* and mediation effects in our primary linear mediation model (similar to the nonparametric analysis above). Results are reported below and included in Tables 2 and 3.

Results

Behavioral analysis

Behavioral relationship between stimulus and report—Pain reports were highly correlated with noxious stimulus intensity: the linear mixed model revealed a significant effect of temperature on pain ($t(25) = 14.45$, $p < 0.001$), such that pain reports increased by 0.73 points on the VAS scale for each unit change in temperature. The linear effect of temperature on pain is modeled as Path *c* in the multi-level mediation analysis (Figure 1A). As shown in Figure 3, there was also substantial variability in this relationship (variance in linear effect of temperature: $M = 1.93$, $SD = 0.75$). We searched for mediators that explained this variance. We also tested nonlinear effects of temperature on pain and found that the relationship was captured by a power law with exponent 2.49, consistent with previous work [65]. We therefore additionally modeled nonparametric effects of temperature for Path *b* and mediator regions below.

Finally, we tested whether the masked emotion faces influenced pain reports. There was no main effect of Masked Emotion (Fear vs Happy) on pain ($p > 0.3$), however there was a significant Temperature *x* Masked Emotion interaction ($t(25) = 3.79$, $p < .001$), such that there was a steeper slope in temperature effects on pain when stimuli were preceded by subliminal fear faces, relative to subliminal happy faces. Because this comparison lacks a neutral control condition and requires replication before we interpret it strongly, we cannot make claims about these effects without replication and extension in additional experiments. Thus, we do not focus on these effects here, but we evaluate whether results reported below remain significant controlling for priming effects due to faces.

Multi-level mediation analysis

The mediation analysis (Figure 1a) included three tests of the links between the objective stimulus and the pain response: 1) Path *a*, stimulus-related responses; 2) Path *b*, pain-related responses, controlling for temperature; and 3) Path *a x b*, mediators of the relationship between stimulus and response, i.e., a formal test of whether the brain region explains a significant amount of the covariance between temperature and pain.

Path a, stimulus-related activity—Increasing temperature produced increases in activation throughout the PPBN, including bilateral insula (with contiguous activation covering anterior, middle and dorsal posterior insula), bilateral secondary somatosensory cortex (SII), right primary somatosensory cortex (SI), bilateral medial thalamus, dorsal anterior cingulate cortex (dACC; with coverage extending to supplementary motor area (SMA) and middle cingulate regions), in the midbrain surrounding the periaqueductal gray (PAG), and bilateral and medial cerebellum (Figure 4A and Table 1). Temperature-related

increases were also found in regions outside of the PPBN, including bilateral lateral orbitofrontal cortex (latOFC), right lateral prefrontal cortex (latPFC), bilateral dorsolateral prefrontal cortex (DLPFC) and right caudate.

Temperature was inversely related to BOLD responses in right dorsomedial prefrontal cortex (DMPFC; superior frontal gyrus), ventromedial prefrontal cortex (VMPFC), bilateral parahippocampal gyrus, bilateral hippocampus, bilateral primary motor cortex (M1), bilateral fusiform gyrus, precuneus, cuneus, subgenual and posterior cingulate cortex, bilateral middle temporal cortex, and bilateral occipital cortex (see Table 1). As we describe below, some of these regions were also related to pain report, and others were not. Path *a* effects on all regions remained significant when Masked Emotion type and the Emotion *x* Temperature interaction were included as covariates.

Path b, pain-related responses—fMRI activity in a number of regions in the *a priori* PPBN mask predicted pain reports, controlling for temperature (Figure 4B and Table 2), including bilateral anterior and middle insula, bilateral SII, right S1, dACC, SMA, right globus pallidus, and bilateral cerebellum. Other regions outside of the PPBN also positively predicted pain, including bilateral DLPFC (middle frontal gyrus), bilateral latOFC (middle orbital gyrus), and bilateral superior parietal lobule (SPL).

BOLD responses were inversely related to pain reports in another set of other areas, including bilateral parahippocampal cortex, right hippocampus, left VMPFC, MPFC, left VLPFC/lateral OFC (inferior frontal gyrus pars orbitalis), rostral anterior cingulate cortex (rACC), pons, cuneus, bilateral temporal pole, right middle and inferior temporal gyrus, posterior cingulate, and bilateral occipital cortex (see Table 2).

Every region that showed significant Path *b* effects remained significant when we used a nonparametric model of temperature, suggesting that these effects were not driven by nonlinearities with respect to temperature (see Table 2). We also evaluated effects controlling for the face primes by modeling Masked Emotion and the Emotion *x* Temperature interaction as covariates (see Table 2). All positive Path *b* effects remained significant when we controlled for the effects of face primes. While most negative Path *b* regions remained significant, Path *b* effects on bilateral temporal pole, rACC, and one cluster in left VLPFC were no longer significant (see Table 2).

Thus, trial-by-trial variations in activity in these regions predicted trial-by-trial variations in report, even when temperature was held constant. As we describe below, some of these regions covaried with stimulus temperature and others did not; in addition, some predicted pain report even when controlling for activity in PPBN mediators.

Path a x b, mediation effect—A number of regions positively mediated the within-subjects relationship between stimulus intensity and reported pain (see Figure 5A and Table 3). Mediation effects in some regions were driven by *consistent* effects—i.e., significant stimulus-related (Path *a*) *and* pain-related effects (Path *b*) across all participants—whereas others were driven by covariance in paths (i.e., correlated individual differences in Path *a*

and Path *b* effects). In either case, positive mediation implies that activity in this region explains some of the effects of noxious heat on reported pain.

Mediator regions that showed consistent effects are illustrated in Figure 3B. In most mediators that fell within the *a priori* PPBN mask, activation both increased with temperature and predicted pain (i.e., positive Path *a* and *b*; red in Figure 5B, Table 3). We observed this pattern of effects in bilateral anterior/mid-insula, bilateral SII, dACC, left cerebellum, right lateral PFC, right SMA (BA6), right superior parietal lobule (SPL), and right premotor cortex. In other mediator regions (blue in Figure 5B, Table 3), temperature increases produced *deactivation*, and greater *deactivation* predicted greater pain. Because both Path *a* and Path *b* are negative, the overall mediation effect is positive. Such effects were found in included bilateral hippocampus and parahippocampus, bilateral inferior temporal gyrus, left medial prefrontal cortex (MPFC), bilateral occipital cortex, right posterior cingulate cortex, left SPL, and precuneus.

Interestingly, most mediators were driven by covariance between paths (see Figure 5A and Table 3), including right parahippocampus, left latOFC, bilateral latPFC, left caudate, left temporal pole, right fusiform, left VLPFC (inferior frontal gyrus), right middle temporal gyrus, bilateral retrosplenial cortex, posterior cingulate, cuneus, left premotor/lateral PFC, left DLPFC, right DMPFC, right SPL, and precuneus. Significant covariance implies systematic heterogeneity across individuals; i.e., some participants show strong Path *a* and Path *b* responses, whereas others are weak on both. Alternatively, there could be inter-individual differences in the qualitative nature of the relationship between fMRI activity and pain: Some subjects show positive relationships with both temperature and pain, whereas others show negative relationships with both, in the same region. This is possible if, e.g., brain activity represents appraisal or attention processes that serve to increase pain in some individuals and mitigate it in others. Thus, these results raise the possibility that different brain models may be appropriate for different groups of individuals.

Finally, we observed negative mediation effects (blue in Figure 5A; see Table 3) in subgenual anterior cingulate/ medial orbitofrontal cortex (mOFC), left midbrain, and bilateral DMPFC (superior frontal gyrus). These findings suggest that some regions contribute to the stimulus-response relationship but show responses that go against the overall behavioral effect. These patterns have been described as suppressive effects in the mediation literature [51], and the interpretation is that the temperature-pain relationship would be *stronger* if activity in these regions were held constant. Regions in which activation is triggered by increases in temperature, but that serve an endogenous regulatory function, would fit this pattern; however, we do not interpret these results strongly here as they were not predicted *a priori*. Finally, mediation effects in all regions remained significant when we controlled for cue effects by including Masked Emotion and Emotion *x* Temperature as covariates in the mediation analysis (see Table 3).

Relationship to stimulus versus response

Among the regions with significant temperature-related effects, some did not show any substantial evidence for correlations with pain report ("*a* not *b* regions"). Regions positively and uniquely related to temperature (yellow in Figure 6) included right dorsal posterior

insula, bilateral thalamus, midbrain surrounding the PAG, right lateral prefrontal cortex, rostral ACC, bilateral lateral OFC, bilateral inferior frontal gyrus, caudal anterior cingulate cortex, and bilateral cerebellum. Regions negatively and uniquely related to temperature (green in Figure 6) included bilateral medial prefrontal cortex, right dorsomedial prefrontal cortex (DMPFC), bilateral primary motor cortex, left S1, precuneus, left hippocampus, bilateral posterior hippocampus/fusiform gyrus, and bilateral occipital lobe. Activity in these regions is likely to reflect early processing of the noxious input.

Regions that predict variations in report but are not affected by changes in noxious input ("*b* not *a* regions", blue/purple in Figure 6) included right mOFC, bilateral DLPFC (BA46), right DMPFC (superior frontal sulcus), bilateral SMA, right pre-SMA, left posterior insula, left posterior parahippocampus, bilateral superior parietal lobule, and bilateral cerebellum. To ensure specificity to pain reports, we also tested whether these "*b* not *a*" regions predicted pain report controlling for evoked responses within PPBN mediator regions. All regions remained significant controlling for PPBN mediator activation (see Table 2), and remained significant controlling for nonlinear effects of temperature. These regions are likely to represent magnitude estimation, attention, decision-making, and other endogenous processes that relate to variation in report but are unaffected by changes in temperature.

Interestingly, we observed qualitative evidence for anterior-to-posterior gradients in several regions, pictured in Figure 6A. In the left insula and ACC, anterior portions were temperature-related, middle regions showed both temperature and pain effects, and posterior regions were pain-related. We found the opposite gradient in left parahippocampus: more posterior portions were temperature-related, whereas anterior parahippocampus was pain-related. Such gradients should be subjected to quantative spatial tests in future studies.

Mediation by network averages

Finally, we used non-metric multi-dimensional scaling (NMDS) to identify networks of mediators expressed similarly across trials and across individuals. We averaged across clusters within each network and tested for mediation to understand the network's functional significance. Three networks showed consistent mediation effects with positive Paths *a* and *b*, shown in the top panel of Figure 7. The first network included bilateral SII; the second network was made up of bilateral anterior and middle insula, dorsal anterior cingulate, right latPFC, right premotor cortex, and right VLPFC; and the third network included bilateral thalamus, left ventral striatum, midbrain/PAG, and bilateral cerebellum. Two other networks showed positive mediation effects with negative Paths *a* and *b*. One network included bilateral parahippocampal cortex, right hippocampus, bilateral middle temporal gyrus / temporoparietal junction (TPJ), bilateral temporal pole, and right posterior hippocampus (Figure 6, bottom) and the other included bilateral retrosplenial cortex/posterior cingulate and inferior parietal lobule (IPL). Networks illustrated in Figure 7 showed evidence of mediation even controlling for all other mediators, suggesting they are the most proximal predictors of temperature effects on pain. Finally, seven more networks were identified with inconsistent positive mediation effects (significant *a***b*, but non-significant Path *a* and/or Path *b* effects), likely driven by covariance (individual differences) and/or heterogeneity of the behavior of the constituent regions. All effects are reported in Table 4.

Discussion

The present study identified brain networks that contribute to the generation of pain in response to noxious stimulation. This provides the first direct evidence that regions within an *a priori* 'pain processing' brain network (PPBN) formally mediate stimulus intensity effects on pain. Our results also reveal complexity that goes beyond a unitary pain-processing system. First, regions outside the PPBN also mediate temperature effects on pain. Second, mediators were grouped into several networks that make separable contributions to pain. Finally, some regions responded selectively to changes in temperature, while others predicted pain without responding to changes in heat.

Pain-processing brain network mediators

Most mediators that showed consistent profiles across individuals fell within *a priori* ROIs, including bilateral SII, aIns, dACC, left cerebellum, IPL, and SPL. These regions showed temperature-related increases *and* predicted subtle variations in pain, controlling for temperature. Previous work has linked activation in some of these regions to variations in reports without changes in stimulus intensity [7; 14; 62; 82]. Our findings reveal that these regions drive fluctuations in pain even when stimulus intensity varies. These trial-by-trial fluctuations are not reducible to nonlinearities in temperature effects on pain [33], but they could reflect sensory variations due to contact with the thermode (which we attempted to minimize), stimulus history [12; 37; 64], or non-nociceptive processes that modify pain, such as fluctuations in attention [14; 46; 62] and regulatory or preparatory mechanisms that reduce pain [22; 77]. Future studies should distinguish among these possibilities and perhaps quantify how much variance in the brain activity-pain relationship is due to each factor.

Network analyses suggest that PPBN mediators comprise distinct somatosensory, paralimbic cortical (anterior cingulate/insula/lateral sensorimotor/frontal), and subcortical (striatal/brainstem/cerebellar) groups. These findings are broadly consistent with separation of lateral sensory/discriminative vs. medial affective/motivational systems [17], but provide an elaborated view. The cortical network we identified includes lateral and medial areas, and the subcortical regions often included in the 'medial pain system' form a separate, coherent network. Thus, the results extend the concept of the unitary 'pain processing' system, and lay a foundation for a) understanding how networks interact during pain genesis, and b) examining how different factors (stimulus types, psychological contexts, or treatments) affect each network.

Mediators not targeted by ascending nociceptive pathways

Regions outside the *a priori* PPBN also mediated pain. We observed temperature- and pain-related increases as well as mediation in right latPFC, right SMA, right SPL, and right premotor cortex. Though not a direct target of the spino-thalamo-cortical pathway, right latPFC (near Brodmann Area 10) has been implicated in previous pain studies [10; 49; 86]. SMA and premotor activation is also commonly observed in imaging studies of neuropathic pain and acute pain in healthy individuals and might be involved in pain-related motor planning [5; 57; 59].

Two core networks, including hippocampal and parahippocampal cortex, anterior pole, TPJ, and the precuneus, mediated stimulus effects on pain by virtue of *deactivation* with increasing heat, the magnitude of which predicted increased pain. These regions are all associated with the 'default mode network' (DMN). They are active at rest and may represent stimulus-independent thought and internally focused mnemonic, visceromotor, and valuation processes [4; 21]. Previous studies have also shown intensity- and pain-related DMN deactivation [48; 69], linking pain with other processes that capture attention and limit internal thought.

While these temperature- and pain-related decreases may reflect pain-related attention-capture, some of these regions might play a more active role in pain inhibition and generation. Existing evidence suggests that hippocampus and parahippocampal cortices can both enhance or decrease pain. Both receive input from SII via the insula [36]. Noxious stimuli reduce activation in the hippocampus [43; 59] and the parahippocampal gyrus [30; 43]. Hippocampal stimulation in animals produces antinociception [50; 53], and placebo analgesia has been associated with parahippocampal increases [26; 42]. However, noxious stimuli can sometimes *increase* hippocampal activation [11; 30], and hippocampal activity has been associated with anxiety-induced hyperalgesia [61] and nocebo-related increases in pain [41]. Disentangling the factors that lead to antinociceptive or pronociceptive responses is an important direction for future research.

Regions preferential to stimulus vs. pain report

Tests of mediation in single voxels provide an important, but partial, view of systems encoding pain. Areas that represent distinct aspects of the experience—i.e., selective relationships with temperature or pain—can provide clues about the dissociability of nociceptive and decision processes and potential neurophysiological targets for the modulation of each. For example, placebo analgesia is associated with widespread changes in responses to noxious stimuli [78]. It is unclear whether any brain circuits reliably encode thermosensory nociceptive responses *without* being affected by the treatment context. This study identified potential thermosensory circuits in subcortical (e.g., PAG and thalamus), sensory cortex, and fronto-cerebellar circuits. These could be related to early nociception, attentional orienting, nocifensive responses, or other processes; whatever the case, they are more strongly related to stimulus intensity than to pain report.

Conversely, several regions were related to pain, but showed no relationship with stimulus intensity. These regions may support the cognitive and affective processes that contribute to pain evaluation, such as magnitude estimation, conceptual representation, and fluctuations in arousal and attention. Medial and lateral OFC have been associated with expected value and outcome expectancy [45; 68]. DLPFC is broadly associated with decision-making and executive function [54; 55], and right DMPFC has been associated with prospection and mental simulation [1; 3]. These systems may be responsible when contextual factors influence pain without affecting nociception (i.e. as a function of decision-making processes).

Previous studies isolated brain regions whose activation during rating predicts variation in pain [9; 44]. An extension of the present work might use mediation to separate regions

whose activation during the *report* period is related to heat, and those whose pain-related responses are related to endogenous variations in reporting-related activity alone. These would be informative probes of activity related to decision-making biases or memory-related processes. Our study was not designed to address reporting-period activity, as motor-related processes would correlate with heat-related processes due to the consistent mapping of increased pain to rightward movement on our scale.

The pattern of temperature- vs. pain pain-related regions provides new evidence on the question of whether these processes are encoded in different circuits. One pioneering fMRI study associated thermosensation with dpIns and pain perception with aINS [29]. We also found that contralateral dpIns showed linear increases with temperature, but did not predict pain. However, the picture is likely to be more complex, as other portions of dpINS predicted pain but did not respond to temperature, replicating recent results [9], and anterior portions of aINS/operculum tracked temperature without predicting pain. In addition, our data appeared to show posterior-anterior gradients in the insula and dACC from pain report to stimulus encoding. Previous studies have found similar gradients in the parietal cortex [6]. These should be replicated and explicitly tested with spatial statistics in future studies.

Future directions

There are several important outstanding questions, including the need for more information on a) specificity of brain responses to pain, b) connections between experimental thermal pain and other types of pain (e.g., inflammatory and neuropathic pain), c) further characterization of complex responses to stimulus intensity and pain (e.g. nonlinearities and temporal dissociations (e.g. [6; 15; 63]), and d) sources of individuals' variability in path effects (i.e. understanding effects on mediators driven by covariance), such as gender differences and relationship to psychological variables (e.g. Fear of Pain, anxiety).

While assessment of these questions is beyond the scope of the current study, the specificity issue deserves discussion. We observed heterogeneity in PPBN responses, suggesting this network contains both thermosensory regions and regions involved in both thermosensation and magnitude estimation. However, we only examined one modality in this study, and cannot determine whether stimulus intensity effects and relationships with subjective reports would be similar in other modalities, or whether the relationships we observed are unique to nociception and pain. AIns and dACC are activated by a range of tasks [9; 31; 85]. One view is that aIns mediates general interoception [27; 28], and dACC and aIns integrate salient external stimuli of all types with internal states [23]. A similar argument has been made for somatosensory regions [58]. Another view is that these regions contain many types of neurons that encode diverse, but specific, processes, including nociception and pain, and indeed, responses within these regions predict pain across individuals with high accuracy [78]. Future research should use mediation to link stimulus intensity with perception across domains and determine the specificity of pathways identified here.

Summary

Pain is generated by a combination of independent networks. Some are involved in nociception and pain in a classic sense: They show graded responses to noxious input, and

responses predict the magnitude of pain. Others show decreases with temperature that predict pain increases, and may be related to mental processes that antagonize (or sometimes promote) pain. Finally, some regions predict pain without responding to noxious input *per se*, and may encode decision-making processes that shape pain evaluation. The networks identified here provide a rich neurophysiological basis for understanding diverse pain-generation processes, and this approach can be extended to stimulus effects on conscious perception in other domains.

Acknowledgments

The authors would like to acknowledge Katherine Dahl and Natalie Johnston for assistance with data collection. Funding provided by NIH RO1 MH076136 and DA027794.

References

1. Abraham A, Schubotz RI, von Cramon DY. Thinking about the future versus the past in personal and non-personal contexts. Brain Research. 2008; 1233:106–119. [PubMed: 18703030]
2. Adair ER, Stevens JC, Marks LE. Thermally induced pain, the Dol scale, and the psychophysical power law. Am J Psychol. 1968; 81(2):147–164. [PubMed: 5747959]
3. Addis DR, Pan L, Vu MA, Laiser N, Schacter DL. Constructive episodic simulation of the future and the past: distinct subsystems of a core brain network mediate imagining and remembering. Neuropsychologia. 2009; 47(11):2222–2238. [PubMed: 19041331]
4. Andrews-Hanna JR. The Brain's Default Network and Its Adaptive Role in Internal Mentation. The Neuroscientist. 2011:1–21.
5. Apkarian AV, Bushnell MC, Treede RD, Zubieta JK. Human brain mechanisms of pain perception and regulation in health and disease. European journal of pain (London, England). 2005; 9(4):463–484.
6. Apkarian AV, Darbar A, Krauss BR, Gelnar PA, Szeverenyi NM. Differentiating cortical areas related to pain perception from stimulus identification: temporal analysis of fMRI activity. J Neurophysiol. 1999; 81(6):2956–2963. [PubMed: 10368412]
7. Atlas LY, Bolger N, Lindquist MA, Wager TD. Brain Mediators of Predictive Cue Effects on Perceived Pain. J Neurosci. 2010; 30(39):12964–12977. [PubMed: 20881115]
8. Atlas LY, Whittington RA, Lindquist MA, Wielgosz J, Sonty N, Wager TD. Dissociable Influences of Opiates and Expectations on Pain. Journal of Neuroscience. 2012; 32(23):8053–8064. [PubMed: 22674280]
9. Baliki MN, Geha PY, Apkarian AV. Parsing pain perception between nociceptive representation and magnitude estimation. J Neurophysiol. 2009; 101(2):875–887. [PubMed: 19073802]
10. Becerra L, Breiter HC, Stojanovic M, Fishman S, Edwards A, Comite AR, Gonzalez RG, Borsook D. Human brain activation under controlled thermal stimulation and habituation to noxious heat: an fMRI study. Magnetic resonance in medicine : official journal of the Society of Magnetic Resonance in Medicine / Society of Magnetic Resonance in Medicine. 1999; 41(5):1044–1057.
11. Bingel U, Quante M, Knab R, Bromm B, Weiller C, et al. Subcortical structures involved in pain processing: evidence from single-trial fMRI. Pain. 2002; 99:313–321. [PubMed: 12237210]
12. Bingel U, Schoell ED, Herken W, Buchel C, May A. Habituation to painful stimulation involves the antinociceptive system. Pain. 2007; 131(1-2):21–30. [PubMed: 17258858]
13. Bollen K, Stine R. Direct and indirect effects: Classical and bootstrap estimates of variability. Sociological methodology. 1990:115–140.
14. Boly M, Balteau E, Schnakers C, Degueldre C, Moonen G, Luxen A, Phillips C, Peigneux P, Maquet P, Laureys S. Baseline brain activity fluctuations predict somatosensory perception in humans. Proc Natl Acad Sci USA. 2007; 104(29):12187–12192. [PubMed: 17616583]

15. Bornhovd K, Quante M, Glauche V, Bromm B, Weiller C, Buchel C. Painful stimuli evoke different stimulus-response functions in the amygdala, prefrontal, insula and somatosensory cortex: a single-trial fMRI study. Brain. 2002; 125(Pt 6):1326–1336. [PubMed: 12023321]
16. Brodersen KH, Wiech K, Lomakina EI, Lin Cs, Buhmann JM, Bingel U, Ploner M, Stephan KE, Tracey I. Decoding the perception of pain from fMRI using multivariate pattern analysis. Neuroimage. 2012; 63(3):1162–1170. [PubMed: 22922369]
17. Brooks J, Tracey I. From nociception to pain perception: imaging the spinal and supraspinal pathways. J Anat. 2005; 207(1):19–33. [PubMed: 16011543]
18. Brown JE, Chatterjee N, Younger J, Mackey S. Towards a Physiology-Based Measure of Pain: Patterns of Human Brain Activity Distinguish Painful from Non-Painful Thermal Stimulation. PLoS ONE. 2011; 6(9):e24124. [PubMed: 21931652]
19. Buchel C, Bornhovd K, Quante M, Glauche V, Bromm B, Weiller C. Dissociable neural responses related to pain intensity, stimulus intensity, and stimulus awareness within the anterior cingulate cortex: a parametric single-trial laser functional magnetic resonance imaging study. J Neurosci. 2002; 22(3):970–976. [PubMed: 11826125]
20. Büchel C, Bornhovd K, Quante M, Glauche V, Bromm B, Weiller C. Dissociable neural responses related to pain intensity, stimulus intensity, and stimulus awareness within the anterior cingulate cortex: a parametric single-trial laser functional magnetic resonance imaging study. J Neurosci. 2002; 22(3):970–976. [PubMed: 11826125]
21. Buckner RL, Andrews-Hanna JR, Schacter DL. The brain's default network: anatomy, function, and relevance to disease. Annals of the New York Academy of Sciences. 2008; 1124:1–38. [PubMed: 18400922]
22. Bushnell MC, Čeko M, Low LA. Cognitive and emotional control of pain and its disruption in chronic pain. Nat Rev Neurosci. 2013; 14(7):502–511. [PubMed: 23719569]
23. Cauda F, Torta DME, Sacco K, Geda E, D'agata F, Costa T, Duca S, Geminiani G, Amanzio M. Shared “Core” Areas between the Pain and Other Task-Related Networks. PLoS ONE. 2012; 7(8):e41929. [PubMed: 22900003]
24. Coghill RC, Eisenach J. Individual differences in pain sensitivity: implications for treatment decisions. Anesthesiology. 2003; 98(6):1312–1314. [PubMed: 12766637]
25. Coghill RC, Sang CN, Maisog JM, Iadarola MJ. Pain intensity processing within the human brain: a bilateral, distributed mechanism. J Neurophysiol. 1999; 82(4):1934–1943. [PubMed: 10515983]
26. Craggs J, Price D, Perlstein W, Verne NicholasG, Robinson M. The dynamic mechanisms of placebo induced analgesia: Evidence of sustained and transient regional involvement. Pain. 2008; 139:660–669. [PubMed: 18804916]
27. Craig AD. How do you feel? Interoception: the sense of the physiological condition of the body. Nat Rev Neurosci. 2002; 3(8):655–666. [PubMed: 12154366]
28. Craig AD. How do you feel — now? The anterior insula and human awareness Nat. Rev Neurosci. 2009; 10:12.
29. Craig AD, Chen K, Bandy D, Reiman EM. Thermosensory activation of insular cortex. Nat Neurosci. 2000; 3(2):184–190. [PubMed: 10649575]
30. Derbyshire SW, Jones AK, Gyulai F, Clark S, Townsend D, Firestone LL. Pain processing during three levels of noxious stimulation produces differential patterns of central activity. Pain. 1997; 73(3):431–445. [PubMed: 9469535]
31. Dosenbach NUF, Visscher KM, Palmer ED, Miezin FM, Wenger KK, Kang HC, Burgund ED, Grimes AL, Schlaggar BL, Petersen SE. A core system for the implementation of task sets. Neuron. 2006; 50(5):799–812. [PubMed: 16731517]
32. Dum RP, Levinthal DJ, Strick PL. The spinothalamic system targets motor and sensory areas in the cerebral cortex of monkeys. J Neurosci. 2009; 29(45):14223–14235. [PubMed: 19906970]
33. Efron, B.; Tibshirani, RJ. An Introduction to the Bootstrap. New York: Chapman and Hall; 1993.
34. Ekman P, Oster H. Facial expressions of emotion. Annual Review of Psychology. 1979; 30(1): 527–554.
35. Friebel U, Eickhoff S, Lotze M. Coordinate-based meta-analysis of experimentally induced and chronic persistent neuropathic pain. NeuroImage. 2011:1–11.

36. Friedman DP, Murray EA, O'Neill JB, Mishkin M. Cortical connections of the somatosensory fields of the lateral sulcus of macaques: evidence for a corticolimbic pathway for touch. J Comp Neurol. 1986; 252(3):323–347. [PubMed: 3793980]
37. Jepma M, Jones M, Wager TD. The dynamics of pain: Evidence for simultaneous site-specific habituation and site-nonspecific sensitization in thermal. pain The journal of pain. In press.
38. Johnstone T, Salomons TV, Backonja MM, Davidson RJ. Turning on the alarm: The neural mechanisms of the transition from innocuous to painful sensation. NeuroImage. 2012; 59(2):1594–1601. [PubMed: 21945794]
39. Kenny D, Korchmaros J, Bolger N. Lower level mediation in multilevel models. Psychological Methods. 2003; 8(2):115–128. [PubMed: 12924810]
40. Kober H, Barrett L, Joseph J, Bliss-Moreau E, Lindquist K, Wager T. Functional grouping and cortical–subcortical interactions in emotion: A meta-analysis of neuroimaging studies. NeuroImage. 2008; 42:998–1031. [PubMed: 18579414]
41. Kong J, Gollub RL, Polich G, Kirsch I, Laviolette P, Vangel M, Rosen B, Kaptchuk TJ. A functional magnetic resonance imaging study on the neural mechanisms of hyperalgesic nocebo effect. J Neurosci. 2008; 28(49):13354–13362. [PubMed: 19052227]
42. Kong J, Gollub RL, Rosman IS, Webb JM, Vangel MG, Kirsch I, Kaptchuk TJ. Brain activity associated with expectancy-enhanced placebo analgesia as measured by functional magnetic resonance imaging. J Neurosci. 2006; 26(2):381–388. [PubMed: 16407533]
43. Kong J, Loggia ML, Zyloney C, Tu P, Laviolette P, Gollub RL. Exploring the brain in pain: activations, deactivations and their relation. Pain. 2010; 148(2):257–267. [PubMed: 20005043]
44. Kong J, White NS, Kwong KK, Vangel MG, Rosman IS, Gracely RH, Gollub RL. Using fMRI to dissociate sensory encoding from cognitive evaluation of heat pain intensity. Hum Brain Mapp. 2006; 27(9):715–721. [PubMed: 16342273]
45. Kringelbach ML. The human orbitofrontal cortex: linking reward to hedonic experience. Nat Rev Neurosci. 2005; 6(9):691–702. [PubMed: 16136173]
46. Kucyi A, Salomons TV, Davis KD. Mind wandering away from pain dynamically engages antinociceptive and default mode brain networks. Proceedings of the National Academy of Sciences. 2013; 110(46):18692–18697.
47. Lindquist MA, Meng Loh J, Atlas LY, Wager TD. Modeling the hemodynamic response function in fMRI: efficiency, bias and mis-modeling. NeuroImage. 2009; 45(1 Suppl):S187–198. [PubMed: 19084070]
48. Loggia ML, Edwards RR, Kim J, Vangel MG, Wasan AD, Gollub RL, Harris RE, Park K, Napadow V. Disentangling linear and nonlinear brain responses to evoked deep tissue pain. PAIN. 2012:1–12.
49. Lorenz J, Cross D, Minoshima S, Morrow T, Paulson P, Casey K. A unique representation of heat allodynia in the human brain. Neuron. 2002; 35(2):383–393. [PubMed: 12160755]
50. Lovick TA. Central Nervous System Integration of Pain Control and Autonomic Function. News in Physiological Sciences. 1991
51. MacKinnon D, Krull J, Lockwood C. Equivalence of the mediation, confounding and suppression effect. Prevention Science. 2000; 1(4):173–181. [PubMed: 11523746]
52. Marquand AF, Howard M, Brammer MJ, Chu C, Coen S, Mourão-Miranda J. Quantitative prediction of subjective pain intensity from whole-brain fMRI data using Gaussian processes. NeuroImage. 2010; 49(3):2178–2189. [PubMed: 19879364]
53. McKenna JE, Melzack R. Analgesia produced by lidocaine microinjection into the dentate gyrus. Pain. 1992; 49(105-112)
54. Miller EK. The prefrontal cortex and cognitive control. Nat Rev Neurosci. 2000; 1(1):59–65. [PubMed: 11252769]
55. Miller EK, Cohen JD. An integrative theory of prefrontal cortex function. Annu Rev Neurosci. 2001; 24:167–202. [PubMed: 11283309]
56. Mogil JS. The genetic mediation of individual differences in sensitivity to pain and its inhibition. Proc Natl Acad Sci USA. 1999; 96(14):7744–7751. [PubMed: 10393892]
57. Moisset X, Bouhassira D. Brain imaging of neuropathic pain. NeuroImage. 2007; 37(Suppl 1):S80–88. [PubMed: 17512757]

58. Mouraux A, Diukova A, Lee MC, Wise RG, Iannetti GD. A multisensory investigation of the functional significance of the “pain matrix”. NeuroImage. 2011; 54:2237–2249. [PubMed: 20932917]
59. Peyron R, García-Larrea L, Grégoire MC, Costes N, Convers P, Lavenne F, Mauguière F, Michel D, Laurent B. Haemodynamic brain responses to acute pain in humans: sensory and attentional networks. Brain. 1999; 122(Pt 9):1765–1780. [PubMed: 10468515]
60. Peyron R, Laurent B, Garcia-Larrea L. Functional imaging of brain responses to pain. A review and meta-analysis (2000) Neurophysiologie clinique = Clinical neurophysiology. 2000; 30(5): 263–288.
61. Ploghaus A, Narain C, Beckmann CF, Clare S, Bantick SJ, Wise RG, Matthews PM, Rawlins JN, Tracey I. Exacerbation of pain by anxiety is associated with activity in a hippocampal network. J Neurosci. 2001; 21(24):9896–9903. [PubMed: 11739597]
62. Ploner M, Lee MC, Wiech K, Bingel U, Tracey I. Prestimulus functional connectivity determines pain perception in humans. Proc Natl Acad Sci USA. 2009; 107(1):355–360. [PubMed: 19948949]
63. Pomares FB, Faillenot I, Barral FG, Peyron R. The ‘where’ and the ‘when’ of the BOLD response to pain in the insular cortex. Discussion on amplitudes and latencies Neuroimage. 2013; 64(C): 466–475.
64. Price DD, Hu JW, Dubner R, Gracely RH. Peripheral suppression of first pain and central summation of second pain evoked by noxious heat pulses. Pain. 1977; 3(1):57–68. [PubMed: 876667]
65. Price DD, McHaffie J, Stein BE. The Psychophysical Attributes of Heat-Induced Pain andTheirRelationships to Neural Mechanisms. journal of Cognitive Neuroscience. 1992; 4(1):1–14. [PubMed: 23967853]
66. Rish I, Cecchi G, Baliki M, Apkarian A. Sparse regression models of pain perception. Brain Informatics. 2010:212–223.
67. Rissman J, Gazzaley A, D'esposito M. Measuring functional connectivity during distinct stages of a cognitive task. NeuroImage. 2004; 23(2):752–763. [PubMed: 15488425]
68. Schoenbaum G, Roesch MR, Stalnaker TA, Takahashi YK. A new perspective on the role of the orbitofrontal cortex in adaptive behaviour. Nat Rev Neurosci. 2009; 10(12):885–892. [PubMed: 19904278]
69. Seminowicz DA, Davis KD. Pain enhances functional connectivity of a brain network evoked by performance of a cognitive task. J Neurophysiol. 2007; 97(5):3651–3659. [PubMed: 17314240]
70. Shattuck DW, Mirza M, Adisetiyo V, Hojatkashani C, Salamon G, Narr KL, Poldrack RA, Bilder RM, Toga AW. Construction of a 3D probabilistic atlas of human cortical structures. Neuroimage. 2008; 39(3):1064–1080. [PubMed: 18037310]
71. Shrout P, Bolger N. Mediation in experimental and nonexperimental studies: New procedures and recommendations. Psychological Methods. 2002
72. Stevens SS. To Honor Fechner and Repeal His Law. Science. 1961; 133:80–86. [PubMed: 17769332]
73. Stone C, Sobel M. The robustness of estimates of total indirect effects in covariance structure models estimated by maximum. Psychometrika. 1990; 55(2):337–352.
74. Thomas CG, Harshman RA, Menon RS. Noise reduction in BOLD-based fMRI using component analysis. NeuroImage. 2002; 17(3):1521–1537. [PubMed: 12414291]
75. Tohka J, Foerde K, Aron AR, Tom SM, Toga AW, Poldrack RA. Automatic independent component labeling for artifact removal in fMRI. NeuroImage. 2008; 39(3):1227–1245. [PubMed: 18042495]
76. Tölle TR, Kaufmann T, Siessmeier T, Lautenbacher S, Berthele A, Munz F, Zieglgänsberger W, Willoch F, Schwaiger M, Conrad B, Bartenstein P. Region-specific encoding of sensory and affective components of pain in the human brain: a positron emission tomography correlation analysis. Ann Neurol. 1999; 45(1):40–47. [PubMed: 9894875]
77. Tracey I, Mantyh PW. The cerebral signature for pain perception and its modulation. Neuron. 2007; 55(3):377–391. [PubMed: 17678852]
78. Wager T, Atlas L, Lindquist M, Roy M, Woo Cw, Kross E. An fMRI-based neurologic signature for physical pain: Supplement. 2013:1–36.

79. Wager TD, Scott DJ, Zubieta JK. Placebo effects on human μ-opioid activity during pain. Proc Natl Acad Sci USA. 2007; 104(26):11056–11061. [PubMed: 17578917]
80. Wager TD, van Ast VA, Hughes BL, Davidson ML, Lindquist MA, Ochsner KN. Brain mediators of cardiovascular responses to social threat, part II: Prefrontal-subcortical pathways and relationship with anxiety. NeuroImage. 2009; 47(3):836–851. [PubMed: 19465135]
81. Wager TD, Waugh CE, Lindquist M, Noll DC, Fredrickson BL, Taylor SF. Brain mediators of cardiovascular responses to social threat: part I: Reciprocal dorsal and ventral sub-regions of the medial prefrontal cortex and heart-rate reactivity: Supplementary material. NeuroImage. 2009; 47(3):821–835. [PubMed: 19465137]
82. Wiech K, Lin Cs, Brodersen KH, Bingel U, Ploner M, Tracey I. Anterior Insula Integrates Information about Salience into Perceptual Decisions about Pain. J Neurosci. 2010; 30(48):16324–16331. [PubMed: 21123578]
83. Willis WD, Westlund KN. Neuroanatomy of the pain system and of the pathways that modulate pain. Journal of clinical neurophysiology : official publication of the American Electroencephalographic Society. 1997; 14(1):2–31. [PubMed: 9013357]
84. Woodrow KM, Friedman GD, Siegelaub AB, Collen MF. Pain tolerance: differences according to age, sex and race. Psychosom Med. 1972; 34(6):548–556. [PubMed: 4644663]
85. Yarkoni T, Poldrack RA, Nichols TE, Van Essen DC, Wager TD. Large-scale automated synthesis of human functional neuroimaging data. Nat Meth. 2011; 8(8):665–670.
86. Zambreanu L, Wise RG, Brooks JCW, Iannetti GD, Tracey I. A role for the brainstem in central sensitisation in humans. Evidence from functional magnetic resonance imaging. Pain. 2005; 114(3):397–407. [PubMed: 15777865]

Summary

We used multi-level mediation analysis to identify regions whose trial-by-trial responses to heat explained variability in the relationship between noxious stimulus intensity and perceived pain.

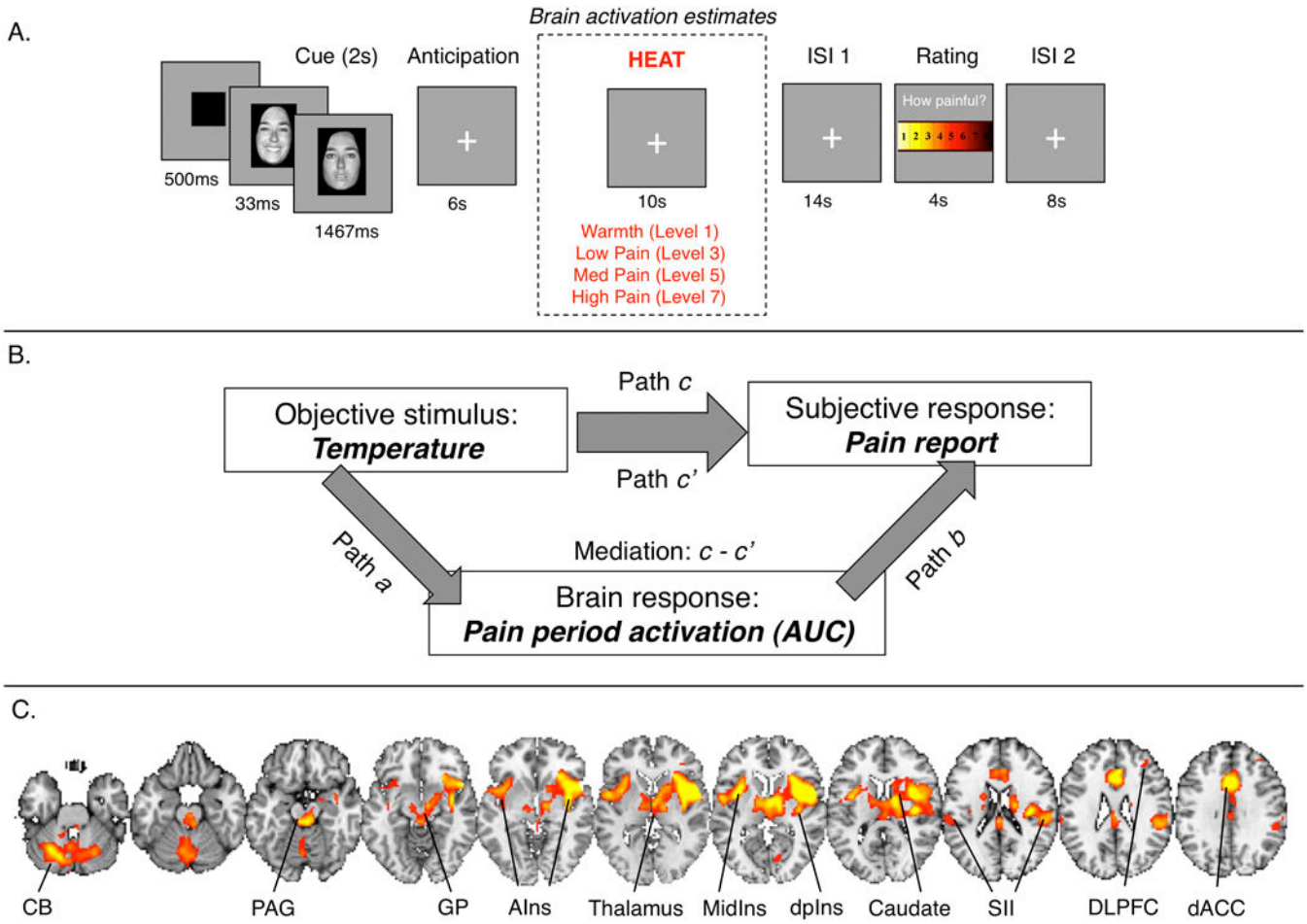

Figure 1. Task and analysis framework

A) *Task design*. On each trial, participants saw a cue, followed by a 6-second anticipatory delay. They then experienced ten seconds of noxious thermal stimulation at temperatures calibrated to elicit ratings of non-painful warmth, low pain, moderate pain, or high pain. Following a delay, participants rated the pain they had experienced. Our analyses examine brain responses during noxious stimulation, using area under the curve (AUC) as a measure of the evoked response. B) M*ulti-level mediation analysis*. Our mediation analyses use linear mixed models to examine the dynamic, trial-by-trial relationship between objective stimulus (Left, X; Temperature), voxelwise stimulus-evoked responses (Bottom, M; AUC estimates from single trial analysis), and pain experience (Right, Y; Pain report). The four components of multilevel mediation analysis address the current study's key questions. Top, Path *c*/*c*′: Does temperature affect perceived pain as measured by trial-by-trial pain reports? Path *c* reflects the total relationship between predictive cue and reported pain on medium trials, and Path *c*′ reflects the direct behavioral relationship, controlling for activity in the mediator—in this case a brain voxel or region. Left, Path *a* (“Temperature effects”) provides inferences on whether brain voxels are modulated by noxious input (Fig. 2A). Right, Path *b* (“report- related responses”) provides inferences on whether brain activity in each voxel predicts trial-by-trial pain reports, controlling for temperature (Fig. 2B). To supplement the standard linear model, we controlled for nonlinear effects of temperature when assessing

Path *b*. Middle, The mediation effect (c – c′) provides inferences on whether brain voxels explain a significant amount of the covariance between temperature and perceived pain (Fig. 3, Fig. 4). C) *Pain-processing brain network*. We were most interested in testing for effects within the *a priori* pain-processing brain network. We created an independent localizer using a mega-analytic approach across four different studies of noxious thermal stimulation (n = 114; see Methods) to identify regions associated with pain and nociception.

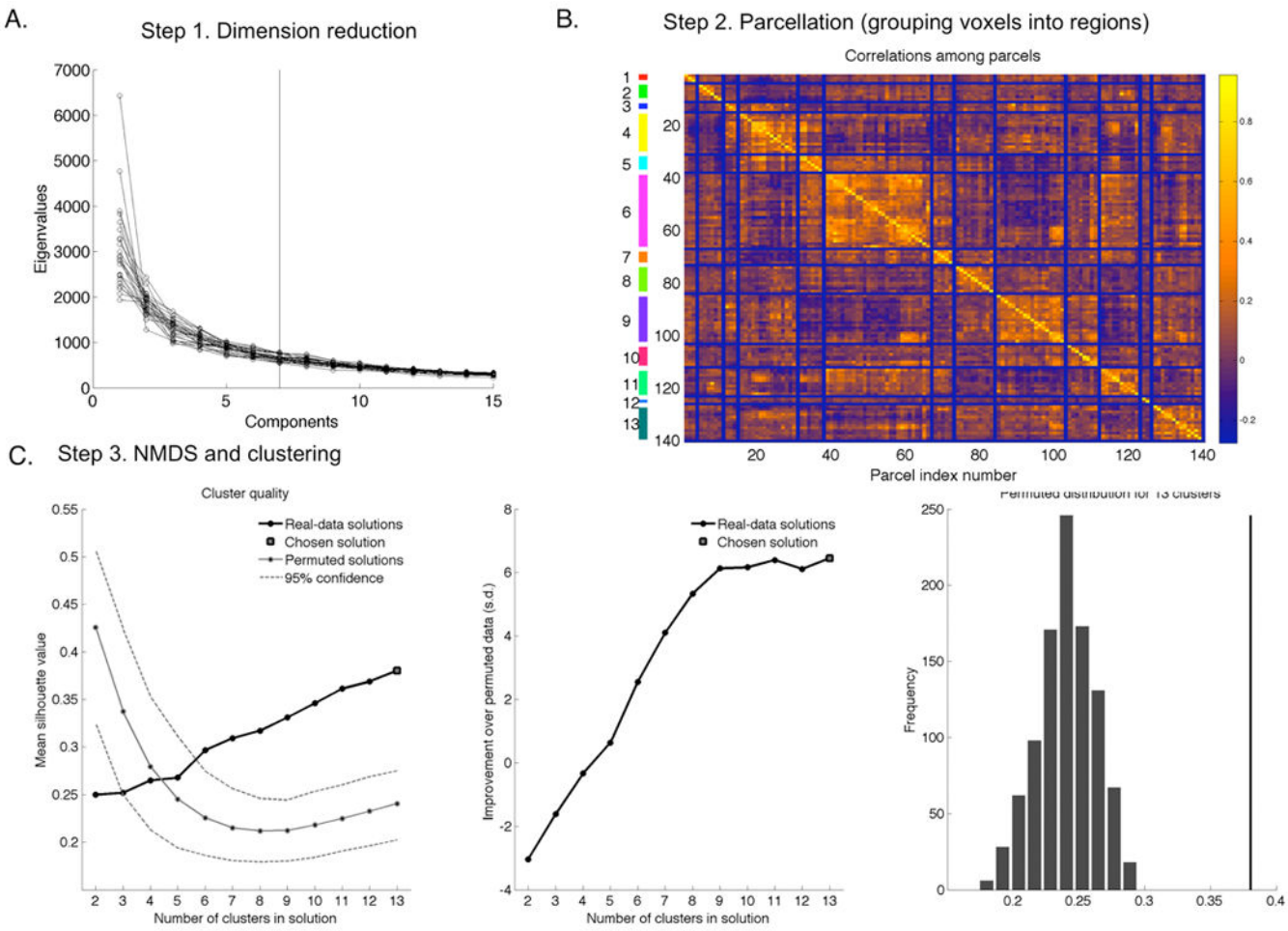

Figure 2. Connectivity analysis

We used a three-step approach to define networks of mediators: A) Step 1: Dimension reduction with principal components analysis; B) Step 2: Parcellation to group voxels into regions; C) NMDS and clustering to identify 13 networks of parcels.

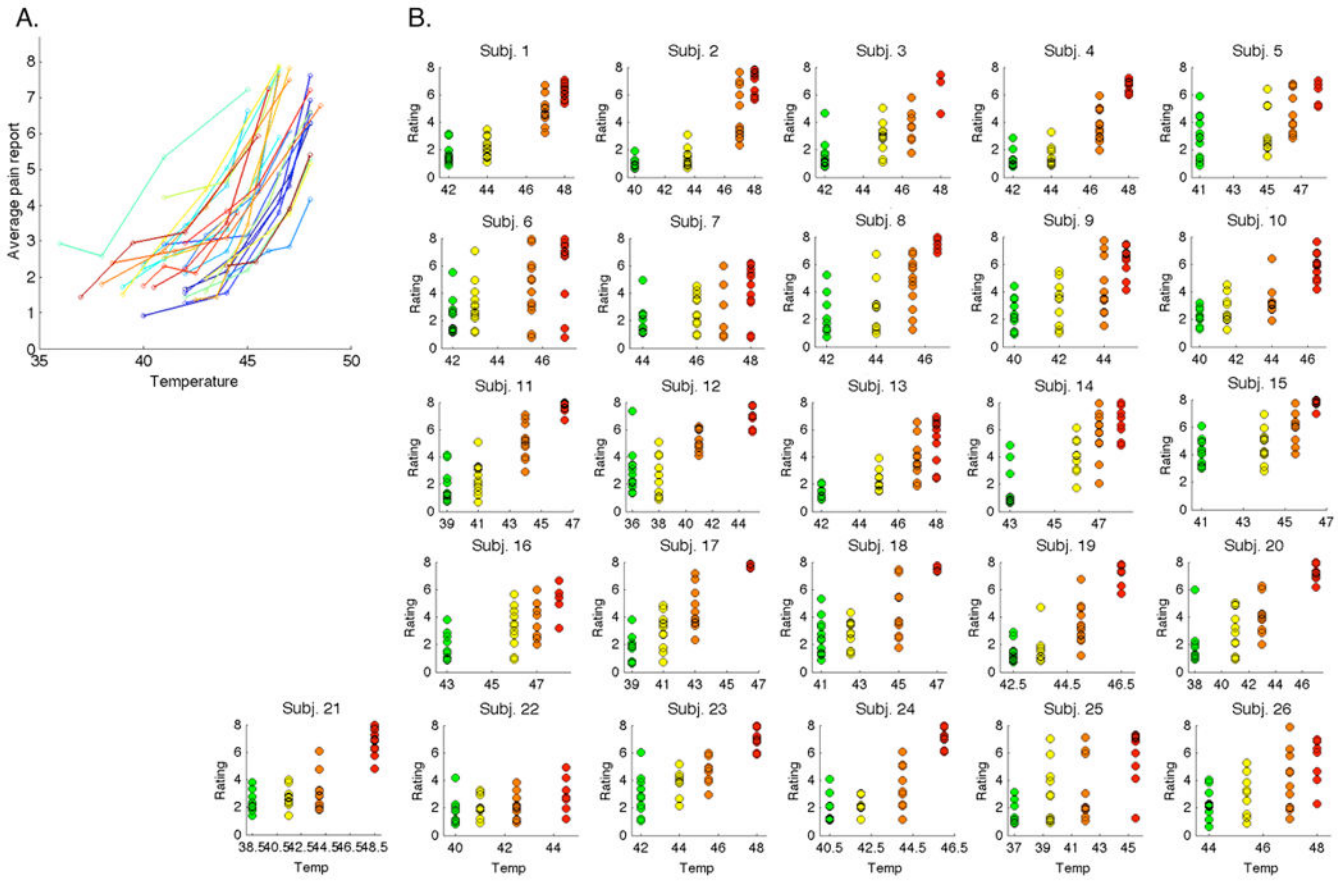

Figure 3. Variability in temperature effects on pain

The relationship between temperature and pain is reliable. However, there is also substantial variability in this relationship both within and between individuals, as demonstrated by plots of each participant's pain ratings as a function of temperature. Mediators help to explain the within-subject variability. A) *Variability across subjects*. Each participant is displayed in a different color. B) *Variability within subjects*. Green = non-painful warmth (calibrated level 1), Yellow = low pain (calibrated level 3), Orange = medium pain (calibrated level 5), Red = high pain (calibrated level 7).

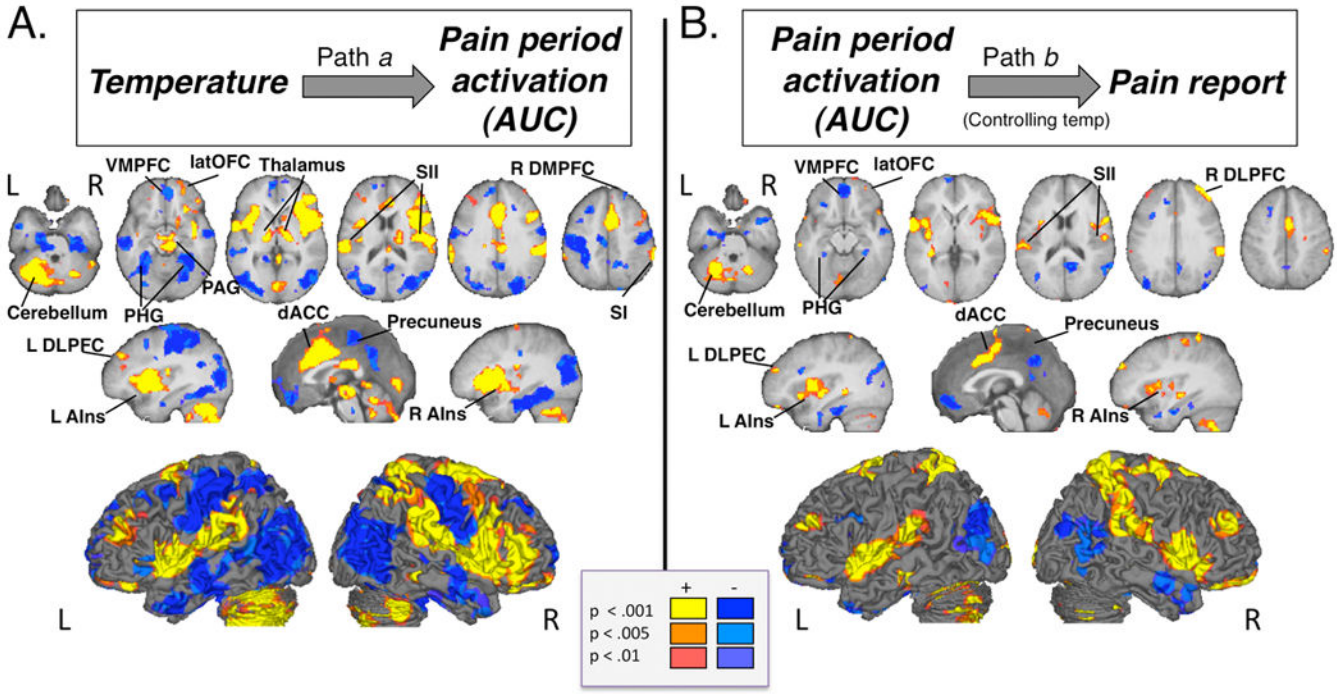

Figure 4. Mediation analysis results

A) Path *a* identifies brain regions that show linear effects of temperature. B) Path *b* identifies brain regions that correlate with pain reports, controlling for temperature. All identified regions were significantly related to trial-by-trial variations in pain using both linear and nonlinear models of temperature-related changes.

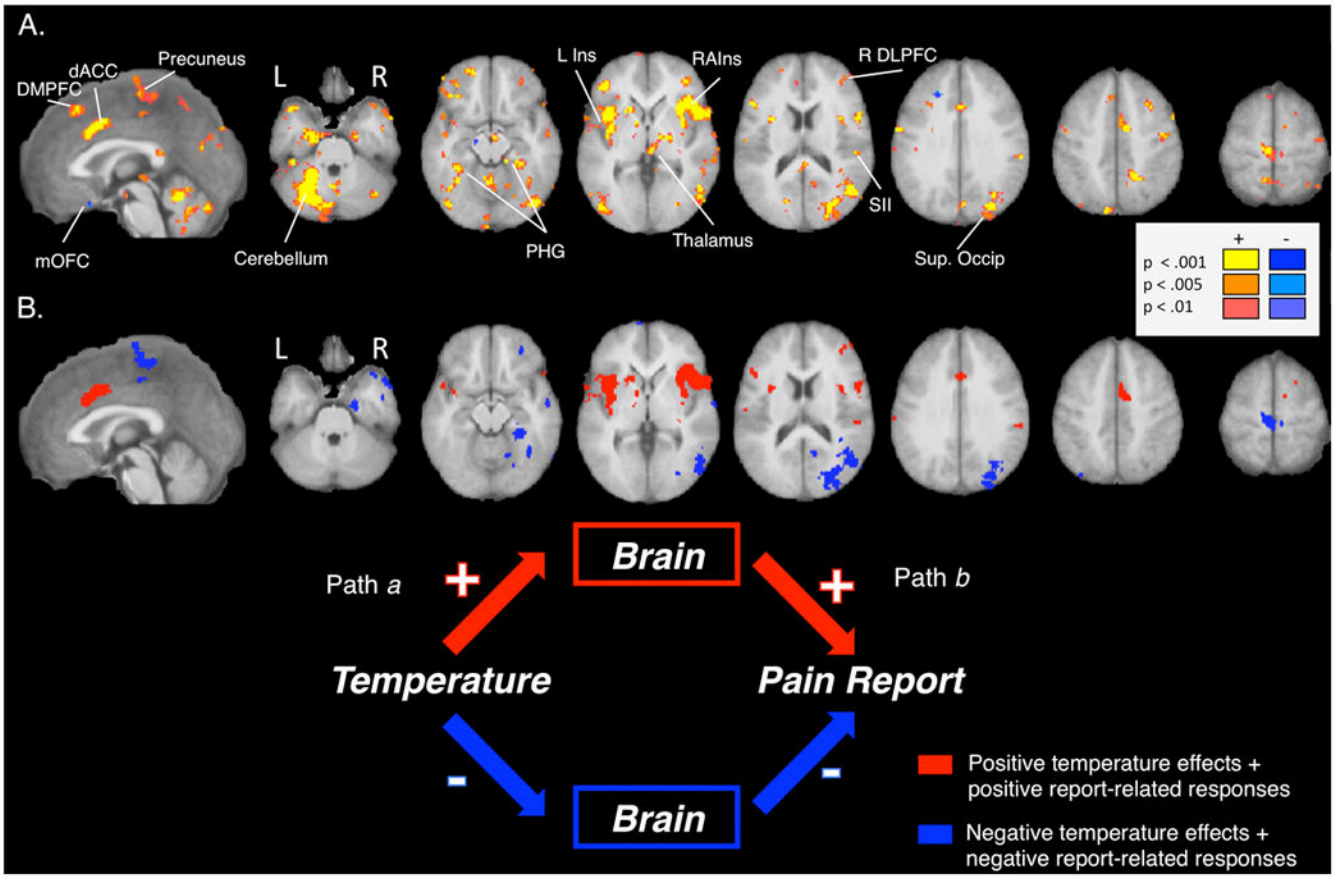

Figure 5. Brain mediators of the relationship between stimulus and response

A) *Mediators of the relationship between temperature and pain.* Brain regions whose responses to noxious stimulation formally mediate the relationship between temperature and pain include those that were activated consistently across the group, as well as those that show covariance between paths. B) *Consistent mediators (significant Path a and Path b effects across subjects).* Regions that were activated consistently across the group include both regions that showed temperature- and pain-related increases, illustrated in red, as well as those that showed temperature- and pain-related decreases, illustrated in blue.

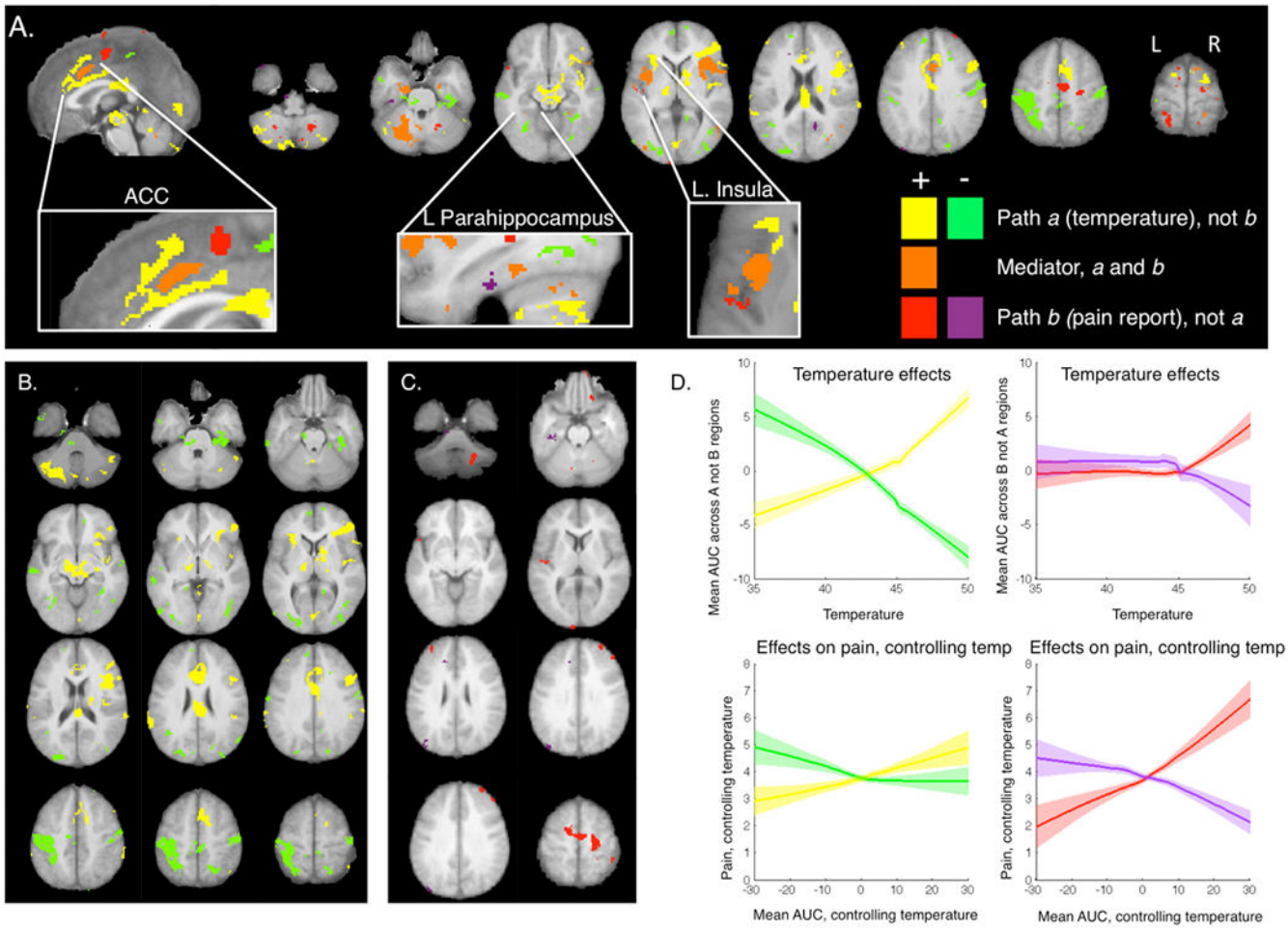

Figure 6. Relationship to stimulus versus response

Regions illustrated in yellow and green were affected by temperature ($p < 0.001$), but were unrelated to pain reports, controlling for temperature ($p > 0.05$) and showed no evidence of mediation ($p > 0 .05$). Blue and purple regions were associated with trial-by-trial pain reports, controlling for temperature ($p < 0.001$), but showed neither temperature-related changes nor mediation (p's > 0.05), and each was significantly related to variations in pain controlling for nonlinear effects of temperature and for activation in PPBN mediators. Mediators that showed consistent effects within subjects, with significant temperature and pain-related effects, are depicted in orange (all paths: $p < .001$). A) We observed anterior-to-posterior gradients in several regions. In the anterior cingulate cortex (ACC; left inset) and left insula (right inset), anterior portions were stimulus-related, middle regions showed activation that was correlated with both increases in stimulus intensity and increases in pain, and posterior regions were related to pain reports. The opposite pattern was observed in left parahippocampus (middle inset): more posterior portions were related to the stimulus, whereas anterior portions were related to pain reports. B) Regions related to temperature but not pain included bilateral medial prefrontal cortex, right dorsomedial prefrontal cortex (DMPFC), bilateral primary motor cortex, left S1, precuneus, left hippocampus, bilateral posterior hippocampus/fusiform gyrus, bilateral occipital lobe, right VMPFC, bilateral

DLPFC (BA46), right SMA, right pre-SMA, left posterior insula, left posterior parahippocampus, and bilateral cerebellum. C) Regions related to pain but not temperature included right mOFC, bilateral DLPFC (BA46), right DMPFC, right SMA, right pre-SMA, left posterior insula, left posterior parahippocampus, and bilateral cerebellum. D) We extracted responses from the regions that showed unique relationships to temperature or pain and averaged across regions and subjects. Loess curves depict responses as a function of applied temperature (top row), and pain as a function of brain response to heat (AUC estimate), controlling for temperature (bottom row). Shaded regions reflect standard error across subjects and therefore should not be used to make inference on random effects.

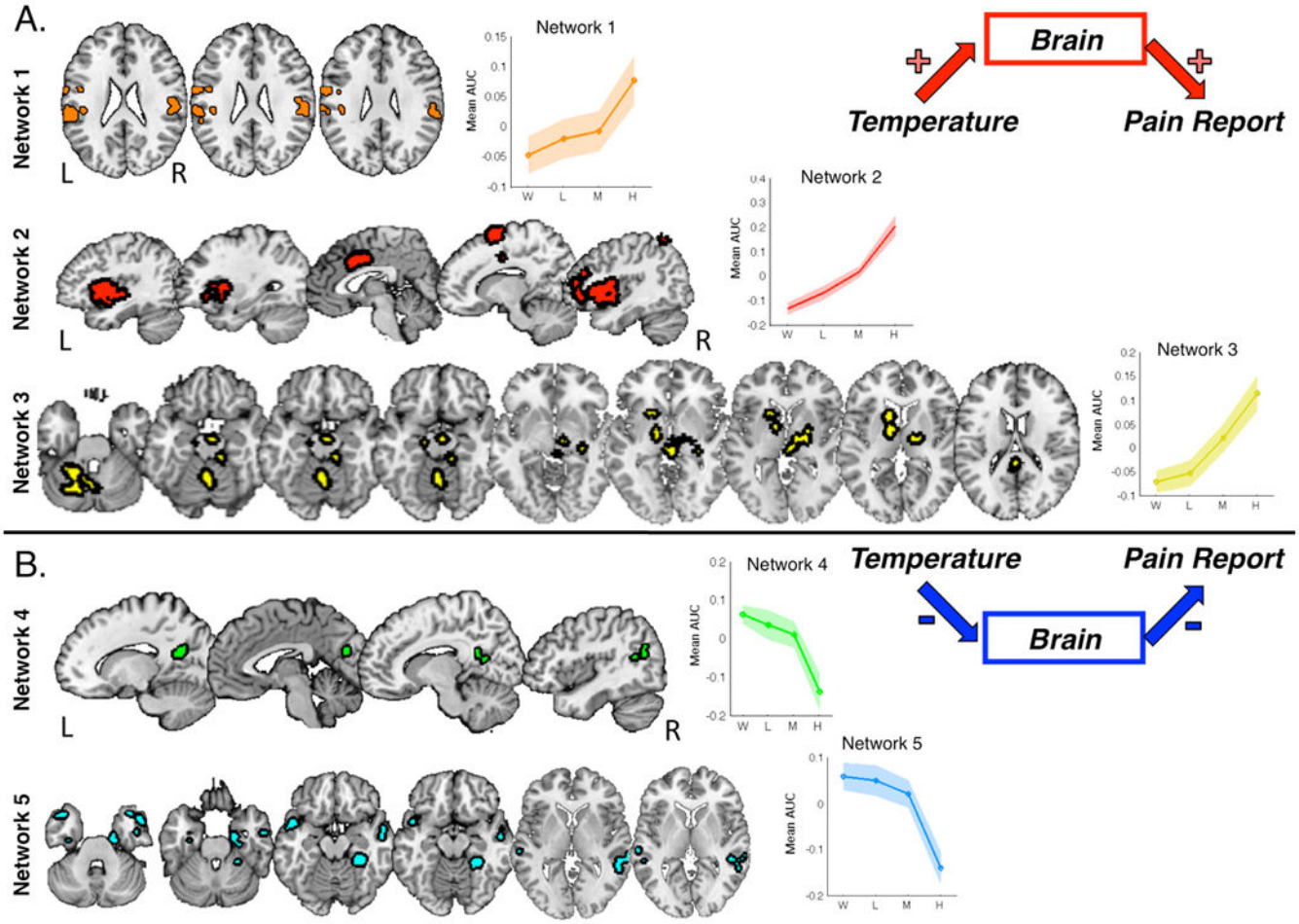

Figure 7. Classes of mediators

We performed nonmetric multi-dimensional scaling to identify networks of mediators, based on functional coactivation within-subjects across trials. Eleven functional networks were identified (see Table 4). *Top:* Three networks consistently showed temperature- and pain-related increases, including a network in bilateral secondary somatosensory cortex (orange), a second network that consisted of bilateral anterior and middle insula, dorsal anterior cingulate, right latPFC, right premotor cortex, and right VLPFC (red), and a third network that included bilateral thalamus, left ventral striatum, midbrain/PAG, and bilateral cerebellum (yellow). Plots of average activation reveal that Networks 2 and 3 were largely linear in relationship to noxious input, whereas Network 1 showed nonlinearities that mirror the behavioral effects of temperature on pain. *Bottom:* Two networks were inversely related to both noxious stimulus and pain reports: one included bilateral retrosplenial cortex / posterior cingulate and inferior parietal lobule (green) and the second included bilateral parahippocampal cortex, right hippocampus, bilateral middle temporal gyrus / temporoparietal junction (TPJ), bilateral temporal pole, and right posterior hippocampus (cyan).

Table 1

Path *a*: Regions correlated with stimulation temperature.[1]

Brain Region (Brodmann Areas)	Coordinates (mm)			# of voxels p<. 001	Volume (mm)	Max Z-score	Mean Path *a* coeff. (std. err)	Mean *p*-value Path *a*
	x	y	z					
Temperature-related increases								
Bilateral cerebellum	-14	-66	-34	6081	48648	15.13	0.9010 (0.17)	0.0000
Right temporal pole	48	-22	-36	6	48	5.86	0.0774 (0.03)	0.0026
Right insula, contiguous with bilateral thalamus, midbrain, right inferior frontal gyrus, right lateral PFC, right premotor cortex, right lateral OFC, right hippocampus	36	2	8	12180	97440	17.22	0.9217 (0.12)	0.0001
Right Inferior Frontal Gyrus p. Orbitalis, contiguous with right anterior insula and right VLPFC	26	14	-24	12	96	5.45	0.4488 (0.17)	0.0087
Left Middle Orbital Gyrus	-26	38	-20	84	672	11.18	0.6833 (0.18)	0.0002
Left Middle Orbital Gyrus	-22	58	-16	38	304	6.26	0.8102 (0.34)	0.0050
Right Middle Temporal Gyrus	58	-40	-10	43	344	8.87	0.4104 (0.12)	0.0006
Left Rolandic Operculum	-46	-4	10	3654	29232	13.63	0.8228 (0.10)	0.0002
Left Calcarine Gyrus (BA17)	2	-84	0	416	3328	10.26	0.9811 (0.25)	0.0003
Right Calcarine Gyrus (BA17)	16	-102	-4	18	144	5.9	0.3819 (0.15)	0.0043
Cerebellar Vermis 4/5	2	-46	-2	106	848	13.82	1.2624 (0.42)	0.0000
Left Insula Lobe (OP2)	-38	-18	14	54	432	12.09	0.4722 (0.13)	0.0001
Right Middle Cingulate Cortex (BA6)	6	6	44	5699	45592	19.94	0.8975 (0.12)	0.0002
Left Middle Frontal Gyrus	-38	42	28	320	2560	10.1	0.7566 (0.17)	0.0016
Right Middle Frontal Gyrus	38	50	28	18	144	5.62	0.8758 (0.30)	0.0037
Left caudal cingulate	-18	-28	34	55	440	8.06	0.4528 (0.13)	0.0003
Left Inferior Parietal Lobule (hIP2)	-44	-42	36	6	48	6.27	0.3704 (0.15)	0.0019
Left Precuneus	-6	-80	54	4	32	5.21	0.5817 (0.25)	0.0100
Left Superior Frontal Gyrus (BA6)	-18	4	66	238	1904	12.39	0.2750 (0.07)	0.0000
Right Superior Parietal Lobule	24	-46	70	367	2936	13.42	0.2867 (0.07)	0.0001
Temperature-related decreases								
Right Medial Temporal Pole	44	12	-42	30	240	6.62	-0.5364 (0.18)	0.0006
Left hippocampus, contiguous with parahippocampal gyrus left medial temporal lobe, left occipital cortex	-34	-54	-8	7155	57240	10.95	-0.7752 (0.10)	0.0006

Brain Region (Brodmann Areas)	Coordinates (mm)			# of voxels p<. 001	Volume (mm)	Max Z-score	Mean Path *a* coeff. (std. err)	Mean *p*-value Path *a*
	x	y	z					
Right hippocampus, contiguous with parahippocampal gyrus and right occipital cortex	40	-64	2	5973	47784	11.59	-0.8269 (0.14)	0.0005
Right Medial Temporal Pole	54	14	-32	2	16	4.87	-0.6793 (0.27)	0.0084
Right Middle Temporal Gyrus	58	-8	-16	429	3432	10.36	-0.9178 (0.21)	0.0001
Right amygdala	14	2	-28	4	32	5.71	-0.4142 (0.14)	0.0016
Left Rectal Gyrus	-6	14	-24	22	176	7.02	-0.3120 (0.09)	0.0005
Right Inferior Temporal Gyrus	66	-24	-26	3	24	5.02	-0.1715 (0.06)	0.0033
Left Superior Medial Gyrus	-4	54	4	1634	13072	9.44	-0.9172 (0.20)	0.0047
Left Rectal Gyrus	-8	24	-14	11	88	5.86	-0.4067 (0.14)	0.0034
Right Cerebelum IV-V	10	-56	-12	4	32	4.86	-0.5879 (0.22)	0.0075
Left Inferior Frontal Gyrus p. Orbitalis	-54	24	-4	42	336	6.96	-0.7147 (0.23)	0.0013
Right Precuneus	2	-44	44	2458	19664	11.26	-0.7598 (0.13)	0.0001
Left Superior Frontal Gyrus	-18	62	2	6	48	5.28	-0.4488 (0.17)	0.0078
Right Superior Temporal Gyrus	44	-28	4	33	264	7.57	-0.3953 (0.11)	0.0002
Right Calcarine Gyrus (BA18)	22	-58	8	13	104	6.52	-0.6114 (0.21)	0.0052
RightPrecentral Gyrus (BA1)	52	-14	46	1377	11016	10.94	-0.7646 (0.15)	0.0004
Left Postcentral Gyrus (BA3b)	-40	-32	52	3869	30952	11.1	-0.7422 (0.13)	0.0014
Right Superior Frontal Gyrus	22	36	38	350	2800	9.41	-0.5574 (0.13)	0.0003
Left Middle Frontal Gyrus	-40	10	50	122	976	7.41	-0.5397 (0.16)	0.0011
Left Middle Frontal Gyrus	-26	24	46	138	1104	8.49	-0.8461 (0.25)	0.0009

[1] *NOTE*: This table presents results from Path *a* of the multi-level mediation analysis presented as a path diagram in Figure 1. Mediation effect parametric mapping results are presented in Figure 3.

*** p < .001

** p < .01

* p < .05

Table 2

Path *b*: Regions correlated with subjective pain, controlling for temperature.[2]

Brain Region (Brodmann Areas)	Coordinates (mm) x	y	z	# of voxels p<.001	Vol (mm)	Max Z-score	Linear temperature effects model: Mean Path *b* coeff. (std. err)	Nonpara-metric temperature effects model: Mean Path *b* coeff. (std. err)	Linear temperature effects, controlling for faces: Mean Path *b* coeff. (std. err)	PPBN mediator independence model: Mean Path *b* coeff. (std. err)
Report-related increases										
Cerebellar Vermis	2	-66	-32	3119	24952	36.04	0.0381 (0.01) ***	0.0283 (0.01) ***	0.0371 (0.01)***	0.0289 (0.01) ***
Right Superior Orbital Gyrus	18	44	-24	310	2480	12.52	0.0163 (0.00) ***	0.0129(0.00) ***	0.0157 (.00) ***	0.0153(0.00) ***
Left lateral OFC	-36	44	-20	58	464	12.19	0.0065 (0.00) ***	0.0064 (0.00) ***	0.0062 (.00)***	0.0067 (0.00) ***
Left Middle Temporal Gyrus	-62	-26	-16	33	264	9.77	0.0051 (0.00) ***	0.0034 (0.00) **	0.0047 (.00)***	0.0077 (0.00) **
Right Middle Orbital Gyrus	32	52	-18	32	256	9.48	0.0036 (0.00) ***	0.0032 (0.00) **	0.0030 (.00)***	0.0025 (0.00) **
Right Insula Lobe	46	10	2	2042	16336	11.07	0.0179 (0.00) ***	0.0150 (0.00) ***	0.0170 (.00)***	0.0068 (0.01) *n.s.*
Left Rolandic Operculum, contiguous with insula	-44	-2	2	2001	16008	14.48	0.0185 (0.00) ***	0.0158 (0.00) ***	0.0178 (.00)***	0.0092 (0.00) *
Right globus pallidus	14	-16	-8	41	328	7.65	0.0095 (0.00) ***	0.0073 (0.00) **	0.0092 (.00)***	0.0037 (0.00) *n.s.*
Left Superior Occipital Gyrus (BA17)	-6	-104	4	72	576	9.14	0.2459 (0.21) ***	0.0785 (0.07) *	0.1983 (.17) **	0.0566 (0.04) **
Left Superior Temporal Gyrus (OP1)	-58	-30	20	428	3424	10.24	0.0117 (0.00) ***	0.0091 (0.00) **	0.0110 (.00)***	0.0014 (0.00) *n.s.*
Right SupraMarginal Gyrus	56	-32	32	1136	9088	13.44	0.0171 (0/00) ***	0.0147 (0.00) ***	0.0165 (.00)***	0.0096 (0.00) *
Right Middle Frontal Gyrus	40	48	30	294	2352	11.21	0.0077 (0.00) ***	0.0074 (0.00) ***	0.0068 (.00)***	0.0039 (0.00) *n.s.*
Left Middle Frontal Gyrus	-36	48	26	111	888	11.42	0.0074 (0.00) ***	0.0074 (0.00) ***	0.0075 (.00)***	0.0046 (0.00) *n.s.*
Right SMA (BA6), contiguous with dACC	8	-14	60	4191	33528	30.8	0.0346 (0.01) ***	0.0244 (0.01) ***	0.0350 (.01)***	0.0227 (0.01) **
Left Superior Parietal Lobule	-24	-50	70	336	2688	36.04	0.0173 (0.01) ***	0.0140 (0.00) **	0.0185 (.01)***	0.0081 (0.00) *n.s.*
Right Superior Parietal Lobule	40	-54	64	42	336	11.44	0.0080 (0.00) ***	0.0076 (0.00) ***	0.0073 (.00)***	0.0040 (0.00) *n.s.*
Report-related decreases										
Left ParaHippocampal Gyrus	-26	-18	-26	724	5792	10.36	-.0229 (0.00) ***	-.0172 (0.00) ***	-0.5456 (.13)***	-.0194 (0.00) ***
Left Temporal Pole	-42	18	-42	54	432	9.29	-.0092 (0.00) ***	-.0091 (0.00) **	-0.2334 (.13) *ns*	-.0060 (0.00) *

Brain Region (Brodmann Areas)	Coordinates (mm) x	y	z	# of voxels p<.001	Vol (mm)	Max Z-score	Linear temperature effects model: Mean Path *b* coeff. (std. err)	Nonpara-metric temperature effects model: Mean Path *b* coeff. (std. err)	Linear temperature effects, controlling for faces: Mean Path *b* coeff. (std. err)	PPBN mediator independence model: Mean Path *b* coeff. (std. err)
Right Medial Temporal Pole	26	16	-38	67	536	7.25	-.0132 (0.00) **	-.0128 (0.00) ***	0.0643 (.12) *ns*	-.0137 (0.00) **
Right Temporal Pole	42	10	-28	169	1352	8.74	-.0090 (0.00) ***	-.0093 (0.00) ***	-0.1961 (.24) *ns*	-.0086 (0.00) **
Right ParaHippocampal Gyrus (Hipp CA)	26	-12	-24	263	2104	9.33	-.0121 (0.00) ***	-.0090 (0.00) ***	-0.6034 (.16) ***	-.0099 (0.00) ***
Right Fusiform Gyrus	30	-36	-14	168	1344	8.85	-.0116 (0.00) ***	-.0087 (0.00) ***	-0.7728 (.18) ***	-.0087 (0.00) **
Right Middle Temporal Gyrus	56	-6	-18	228	1824	9.16	-.0080 (0.00) ***	-.0066 (0.00) ***	-0.8675 (.24) ***	-.0068 (0.00) ***
Left Mid Orbital Gyrus, contiguous with MPFC (VMPFC)	-2	54	-10	684	5472	10.62	-.0083 (0.00) ***	-.0073 (0.00) ***	-1.1621 (.32) **	-.0057 (0.00) *
Right Middle Temporal Gyrus	54	-66	16	649	5192	9.11	-.0181 (0.00) ***	-.0165 (0.00) ***	-0.5814 (.15) ***	-.0140 (0.00) **
Left Inferior Frontal Gyrus p. Orbitalis	-28	32	-12	49	392	8.4	-.0068 (0.00) ***	-.0044 (0.00) **	-0.1378 (.16) *ns*	-.0073 (0.00) ***
Left Middle Occipital Gyrus	-40	-80	22	752	6016	10.35	-.0135 (0.00) ***	-.0110 (0.00) ***	-0.6046 (.16) ***	-.0113 (0.00) ***
Right Precuneus	4	-56	26	985	7880	11.02	-.0092 (0.00) ***	-.0089 (0.00) ***	-0.7416 (.22) **	-.0057 (0.00) *
Left rostral ACC	-16	32	26	111	888	8.88	-.0120 (0.00) ***	-.0012 (0.00) ***	0.1080 (.15) *ns*	-.0160 (0.00) ***
Left Inferior Frontal Gyrus p. Triangularis	-38	18	26	127	1016	8.13	-.0122 (0.00) **	-.0092 (0.00) **	-0.1411 (.18) *ns*	-.0121 (0.00) **
Left Middle Frontal Gyrus	-24	20	44	162	1296	9.12	-.0095 (0.00) ***	-.0077 (0.00) ***	-0.4318 (.19) *	-.0063 (0.00) *n.s.*

[2] *NOTE*: This table presents results from Path *b* of the multi-level mediation analysis presented as a path diagram in Figure 1. Mediation effect parametric mapping results are presented in Figure 3.

*** p < .001

** p < .01

* p < .05

Table 3

Path $a^{*}b$: Brain mediators of temperature effects on pain.[3]

Brain Region (Brodmann Areas)	Coordinates (mm)			# of voxels p<. 001	Vol (mm)	Mea *a x b* (std. err)	Cov (a, b)	Path *a* and Path *b effects*, if consistent across individuals	Nonpara-metric temperature effects model: Mean Path ab coeff. (std. err)	Mediation effect controlling for faces: Mean Path *ab* coeff. (std. err)
	x	y	z							
Positive Mediators										
Right Cerebelum Crus 2	52	-52	-44	108	864	0.004 (0.001)***	0.014		0.006 (0.002)*	0.0042 (.00)***
Right Cerebelum VIII	28	-60	-48	61	488	0.003 (0.001)***	-0.104		0.003 (0.001)*	0.0041 (.00)***
Left Parahippocamp al gyrus, contiguous with left cerebellum	-24	-52	-26	4422	35376	0.005 (0.001)***	0.023		0.007 (.002)*	0.0064 (.00)***
Left Medial Temporal Pole	-36	14	-36	85	680	0.006 (0.002)***	0.023		0.014 (.003)**	0.0067 (.00)***
Right temporal pole	48	-12	-46	15	120	0.002 (0.000)**	0.012		0.004 (0.001)**	0.0026 (.00)***
Left temporal pole	-34	-20	-42	20	160	0.004 (0.001)**	0.017		0.005 (0.002)*	0.0044 (.00)***
Right Fusiform Gyrus	36	-12	-40	16	128	0.002 (0.001)**	0.011		0.005 (0.002)*	0.0044 (.00)***
Right Medial Temporal Pole	50	12	-26	461	3688	0.003 (0.001)*	0.008	Negative a, Negative b	0.007 (0.002)**	0.0041 (.00)*
Right Hippocampus, parahippocamp us, Fusiform Gyrus	28	-40	-16	749	5992	0.005 (0.002)***	0.005	Negative a, Negative b	0.007 (0.003)*	0.0079 (.00)***
Right Inferior Occipital Gyrus	40	-74	-16	319	2552	0.007 (0.001)**	0.025		0.006 (0.002)*	0.0083 (.00)***
Left Superior Orbital Gyrus	-12	30	-22	14	112	0.003 (0.001)***	0.015		0.004 (0.001)**	0.0040 (.00)***
Left Inferior Frontal Gyrus p. Orbitalis, contiguous with left MPFC, rACC	-36	40	-4	805	6440	0.007 (0.001)***	0.027		0.009 (0.002 ***	0.0089 (.00)***
Right Rectal Gyrus	6	32	-20	29	232	0.003 (0.001)***	0.014		0.007 (0.002)*	0.0034 (.00)***
Left Calcarine Gyrus (BA18)	-6	-94	-10	129	1032	0.006 (0.002)***	0.013		0.005 (0.002)*	0.0078 (.00)***
Right Cerebelum III	14	-32	-16	30	240	0.002 (0.001)**	0.011		0.006 (0.002)***	0.0043 (.00)***
Left Middle Orbital Gyrus	-20	54	-16	94	752	0.006 (0.001)***	0.02		0.006 (0.002)**	0.0072 (.00)***
Midbrain, hypothalamus	4	-12	-16	29	232	0.003 (0.001)***	0.004		0.003 (0.002) *n.s.*	0.0050 (.00)***
Left Insula Lobe, contiguous with caudate, putamen, left globus pallidus	-36	8	2	1702	13616	0.013 (0.002)***	0.011	Positive a, Positive b	0.023 (0.003)**	0.0150 (.00)***

Brain Region (Brodmann Areas)	Coordinates (mm)			# of voxels p<. 001	Vol (mm)	Mea *a* x *b* (std. err)	Cov (a, b)	Path *a* and Path *b effects*, if consistent across individuals	Nonpara-metric temperature effects model: Mean Path ab coeff. (std. err)	Mediation effect controlling for faces: Mean Path *ab* coeff. (std. err)
	x	y	z							
Right Insula Lobe	42	14	2	1971	15768	0.017 (0.03)***	0.012	Positive a, Positive b	0.030 (0.004)***	0.0178 (.00)***
Right Middle Occipital Gyrus	36	-74	16	1686	13488	0.009 (0.002)***	0.009	Negative a, Negative b	0.015 (0.003)***	0.0103 (.00)***
Right Middle Orbital Gyrus	46	52	-8	30	240	0.006 (0.002)***	0.022		0.006 (0.002)**	0.0063 (.00)***
Right Thalamus	12	-14	0	220	1760	0.006 (0.002)***	0.011		0.010 (0.004)*	0.0081 (.00)***
Right lateral PFC	38	42	-2	122	976	0.005 (0.001)***	0.014		0.004 (0.001)**	0.0056 (.00)***
Right Middle Temporal Gyrus	58	-36	2	113	904	0.002 (0.001)*	0.012		0.004 (0.001)**	0.0030 (.00)*
Left Superior Medial Gyrus	-10	70	6	42	336	0.003 (0.001)**	0.009	Negative a, Negative b	0.006 (0.002)**	0.0055 (.00)***
Left Superior Temporal Gyrus	-62	-24	4	11	88	0.003 (0.001)***	0.005		0.006 (0.002)***	0.0046 (.00)***
Area 17	-26	-72	6	19	152	0.003 (0.001)**	0.011		0.005 (0.002)**	0.0044 (.00)***
Left Middle Temporal Gyrus	-56	-38	8	22	176	0.002 (0.001)***	0.004		0.003 (0.001)*	0.0031 (.00)*
Right Middle Frontal Gyrus	44	42	20	119	952	0.004 (0.001)*	0.008	Positive a, Positive b	0.004 (0.001)**	0.0056 (.00)***
Right Precuneus	12	-52	18	57	456	0.002 (0.001)***	0.005	Negative a, Negative b	0.004 (0.002) *n.s.*	0.0035 (.00)***
Right SII, SupraMarginal Gyrus	56	-24	24	139	1112	0.005 (0.001)***	0.005	Positive a, Positive b	0.005 (0.001)***	0.0069 (.00)***
Posterior cingulate cortex	0	-40	18	29	232	0.002 (0.000)***	0.008		0.004 (0.001)*	0.0038 (.00)***
Left Cuneus	-4	-84	34	328	2624	0.004 (0.001)***	0.017		0.002 (0.002) *n.s.*	0.0061 (.00)***
Left Cuneus	-14	-56	22	75	600	0.002 (0.001)***	0.008		0.008 (0.001) *n.s.*	0.0040 (.00)***
Left SII, SupraMarginal Gyrus	-58	-30	24	127	1016	0.006 (0.002)***	0.009	Positive a, Positive b	0.008 (0.002)**	0.0078 (.00)***
Left Postcentral Gyrus (Area 3b)	-60	-4	28	65	520	0.005 (0.001)***	0.014		0.007 (0.003)**	0.0063 (.00)***
Left Precentral Gyrus	-48	-2	24	14	112	0.003 (0.001)***	0.008		0.003 (0.001)*	0.0041 (.00)**
Left Middle Frontal Gyrus	-30	22	30	20	160	0.003 (0.001)***	0.013		0.001 (0.001) *n.s.*	0.0029 (.00)*
Right Middle Cingulate Cortex	4	10	40	434	3472	0.013 (0.003)***	0.006	Positive a, Positive b	0.016 (0.005)**	0.0156 (.00)***
Right Superior Frontal Gyrus	20	22	38	29	232	0.003 (0.001)***	0.009		0.004 (0.001)*	0.0040 (.00)***

Pain. Author manuscript; available in PMC 2015 August 01.

Brain Region (Brodmann Areas)	Coordinates (mm)			# of voxels p<.001	Vol (mm)	Mea *a x b* (std. err)	Cov (a, b)	Path *a* and Path *b effects*, if consistent across individuals	Nonpara-metric temperature effects model: Mean Path ab coeff. (std. err)	Mediation effect controlling for faces: Mean Path *ab* coeff. (std. err)
	x	y	z							
Left Superior Medial Gyrus	-4	26	52	198	1584	0.004 (0.001)***	0.014		0.013 (0.003)***	0.0062 (.00)***
Left Precentral Gyrus (BA6)	-54	-2	46	69	552	0.004 (0.001)***	0.007		0.005 (0.002)**	0.0048 (.00)***
RightPrecentral Gyrus (BA6)	48	-10	52	226	1808	0.006 (0.002)***	0.012		0.008 (0.004) *n.s.*	0.0072 (.00)**
RightPrecentral Gyrus	52	8	50	70	560	0.005 (0.001)***	0.013		0.007 (0.002)**	0.0082 (.00)***
Right Middle Frontal Gyrus	32	22	44	40	320	0.002 (0.001)**	0.006		0.001 (0.001) *n.s.*	0.0035 (.00)**
Left Superior Parietal Lobule	-34	-70	52	70	560	0.003 (0.001)***	0.009	Negative a, Negative b	0.002 (0.002) n.s.	0.0046 (.00)***
Left Paracentral Lobule (BA4a)	0	-24	66	598	4784	0.008 (0.002)***	0.016	Negative a, Negative b	0.009 (0.005)*	0.0106 (.00)***
Left Precuneus	-2	-56	60	141	1128	0.003 (0.001)***	0.013		0.005 (0.002)*	0.0050 (.00)***
Right Superior Parietal Lobule	38	-58	64	74	592	0.002 (0.001)***	0.006		0.004 (0.002)*	0.0047 (.00)***
Left Precuneus	-14	-72	62	9	72	0.002 (0.000)***	0.006		0.001 (0.001) *n.s.*	0.0029 (.00)**
Right SMA (BA6)	14	8	68	297	2376	0.006 (0.002)***	0.038	Positive a, Positive b	0.004 (0.002)*	0.0081 (.00)***
Right Postcentral Gyrus (BA1)	24	-42	68	70	560	0.005 (0.001)***	0.003	Positive a, Positive b	0.010 (0.003)***	0.0072 (.00)***
Left Precuneus	-10	-66	66	6	48	0.002 (0.001)***	0.008		0.003 (0.002) n.s.	0.0030 (.00)**
RightPrecentral Gyrus	26	-14	70	68	544	0.005 (0.001)***	0.013	Positive a, Positive b	0.002 (0.002) n.s.	0.0065 (.00)***
Negative Mediators										
Left Rectal Gyrus	65	-2	18	-24	15	-0.002 (0.001)***	0.000		-0.003 (0.002)*	-0.0028 (.00)**
Left midbrain, hippocampus	66	-16	-16	-14	10	-0.001 (0.000)***	-0.006		-0.003 (0.001)***	-0.003 (.00)***
Left Superior Frontal Gyrus	68	-22	32	30	21	-0.002 (0.001)***	-0.001		-0.004 (0.001)**	-0.004 (.00)***
Right Middle Frontal Gyrus	69	26	48	36	22	-0.009 (0.001)***	-0.008		-0.004 (0.002)**	-0.005 (.00)***

[3] *NOTE*: This table presents results from Path *a*b* of the multi-level mediation analysis presented as a path diagram in Figure 1. Mediation effect parametric mapping results are presented in Figure 4.

*** p < .001

** p < .01

* $p < .05$

Table 4

Mediator networks and relationship to temperature effects on pain.[4]

Network components	Path *a*	Path *b*	Path *c*	Path *c′*	Mediation (c-c′)
Consistent mediator networks: Positive path coefficients					
Network 1: Bilateral SII, M1	2.148*	2.387*	3.933***	3.953***	3.144**
Network 2: Bilateral anterior insula, Bilateral middle insula, dACC, R DMPFC, bilateral precentral gyrus, R latPFC, R VLPFC, R SPL	3.747***	3.635***	3.652***	3.967***	3.586***
Network 3: Right thalamus, PAG, midbrain, medial cerebellum, left ventral striatum, ventral striatum, right globus pallidus	3.570***	2.213*	4.040***	3.988***	3.078**
Consistent mediator networks: Negative path coefficients					
Network 4: Bilateral retrosplenial cortex, R IPL	-3.313***	-3.551***	3.979***	3.921***	3.720***
Network 5: Bilateral hippocampus, R parahippocampus, bilateral middle temporal gyrus / TPJ, bilateral temporal operculum, L IFG	-3.236***	-1.784⊥	3.937***	3.920***	3.572***
Inconsistent mediators: a,b covariance-driven mediation					
Network 6: Bilateral VMPFC	-0.8142	-0.196	3.900***	3.957***	2.826**
Network 7: Bilateral VLPFC, L IFG	0.564	0.266	3.984***	3.942***	3.677***
Network 8: Bilateral cerebellum, bilateral latOFC, DMPFC, R DMPFC, L SPL	1.930⊥	0.960	3.859***	3.917***	3.084**
Network 9: Bilateral temporal pole, L anterior PFC, L parahippocampal gyrus	-2.472*	-1.587	3.910***	3.935***	3.143**
Network 10: Bilateral occipital cortex, posterior parahippocampal cortex, precuneus, R M1	-3.814***	-0.708	3.923***	3.943***	2.457*
Network 11: L pons, cuneus	-0.706	-0.531	3.935***	3.944***	3.125**

[4] *NOTE*: Results of mediation analysis testing whether average network activation mediates temperature effects on pain reports. Path a: temperature effects. Path b: prediction of pain reports, controlling for temperature. Values reflect z-scores for each effect.

*** $p < .001$

** $p < .01$

* $p < .05$

⊥ $p < .10$